

Recurrent neural chemical reaction networks trained to switch dynamical behaviours through learned bifurcations

Alexander Dack¹

Tomislav Plesa²

Thomas E. Ouldridge¹

Keywords: Chemical Reaction Networks; Dynamical Systems; Artificial Neural Networks.

Abstract: Both natural and synthetic chemical systems not only exhibit a range of non-trivial dynamics, but also transition between qualitatively different dynamical behaviours as environmental parameters change. Such transitions are called bifurcations. Here, we show that recurrent neural chemical reaction networks (RNCRNs), a class of chemical reaction networks based on recurrent artificial neural networks that can be trained to reproduce a given dynamical behaviour, can also be trained to exhibit bifurcations. First, we show that RNCRNs can inherit some bifurcations defined by smooth ordinary differential equations (ODEs). Second, we demonstrate that the RNCRN can be trained to infer bifurcations that allow it to approximate different target behaviours within different regions of parameter space, without explicitly providing the bifurcation itself in the training. These behaviours can be specified using target ODEs that are discontinuous with respect to the parameters, or even simply by specifying certain desired dynamical features in certain regions of the parameter space. To achieve the latter, we introduce an ODE-free algorithm for training the RNCRN to display designer oscillations, such as a heart-shaped limit cycle or two coexisting limit cycles.

1 Introduction

It is common to observe biological entities transition between dynamical behaviours as they process information from their environment [1] or as they proceed through their developmental cycle [2]. For example, it is well-known in cellular biology that cells differentiate, i.e. change type, to specialise into particular functions [3]. Expressed in the nomenclature of dynamical systems, cells are moving between different dynamical regimes capable of different behaviours that govern their function. In some dynamical systems, it is external factors, called *parameters*, that determine the dynamical regime. In biochemistry, such parameters may be interpreted as the reaction rate coefficients or the concentrations set by exogenous chemostat.

Switching of dynamical behaviours as parameters are changed is studied in a branch of mathematics called *bifurcation theory* [4]. This general theory has categorized the types of transitions into canonical forms [4] and been applied broadly to understand a range of biological phenomena including snapping mechanism in the Venus fly trap [5], predator-prey relationships in ecosystems [6], and to model neural networks in the brain [7–11]. Of particular relevance to this work is the investigation of cellular regulation at the biochemical level through the lens of bifurcation theory [12–16].

Aside from being used to model natural biological phenomena, dynamical systems are also used in the fields of synthetic biology and nucleic-acid nanotechnology, which have been successful at engineering biological systems with desired dynamical behaviours. Examples include neural network classification algorithms [17–24] and attractor orbits [25–27], which have been built in a range of

¹Department of Bioengineering and Imperial College Centre for Synthetic Biology, Imperial College London, Exhibition Road, London SW7 2AZ, UK. Email of co-corresponding authors: alex.dack14@imperial.ac.uk or t.ouldridge@imperial.ac.uk.

²Department of Applied Mathematics and Theoretical Physics, University of Cambridge, Centre for Mathematical Sciences, Wilberforce Road, Cambridge, CB3 0WA, UK.

molecular media. Given that individual dynamical behaviours have been realised successfully, a natural question arises: can one combine these components to engineer biological systems with the complicated switching behaviour, or bifurcations, seen in the native systems?

In this context, on the one hand, some research has focused on eliminating undesirable bifurcations in engineered systems [28, 29], and studying how sudden and unexpected changes in dynamical behaviours can lead to catastrophic system failures [30]. For example, such bifurcations are known to lead to hazardous events in synthetic biology control systems [31]. On the other hand, there has also been a growing interest in bifurcation-inspired design paradigms [32, 33], given that bifurcations are potentially a highly efficient solution to achieving large changes in output for only a small change in input. Indeed, there has been both experimental [34, 35] and theoretical work [36–42] investigating the construction of bifurcations in biochemical systems. In particular, mathematical methods for designing *chemical reaction networks* (CRNs), mathematical models of chemistry, that implement a given bifurcation are developed in [43, 44]. All of these methods take as input a sufficiently smooth dynamical system with desired bifurcation structure, which is then converted into a CRN [31, 45–50].

In this paper, we present methods to construct CRNs that use bifurcations to interpolate between regions of desired dynamics, for which only the desired dynamics need to be specified ahead of training. In particular, we base our methods on the *recurrent neural chemical reaction network* (RNCRN) - a class of CRNs that operates as a recurrent neural network, whose fast-acting chemical perceptrons can be trained to approximate arbitrary dynamics [51].

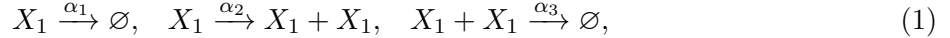
We first demonstrate that the RNCRN with sufficiently many species can be adapted for training to reproduce classical bifurcations from a given smooth parameter-dependent dynamical system, in line with the capabilities of more minimal methods [43, 44]. We then demonstrate that the RNCRN can be further adapted and trained to approximate and merge different behaviours from a given dynamical system which depends on its parameters discontinuously. Finally, we introduce an algorithm for training the RNCRN to approximate limit cycles specified only by the shape of the limit cycle itself, rather than via ODEs that generate a limit cycle, which enables the construction of a variety of behaviours from sparse data. Motivated by the success of chemical classifiers [52–60], we use this algorithm to develop an extended RNCRN that can sense its local environment, perform a non-linear classification, and then toggle between dynamical regimes accordingly. We note that these discontinuous and sparsely defined target systems showcase the RNCRN’s ability to extrapolate outside, and interpolate between, training data to create a self-consistent vector field that matches the intended dynamical behaviour.

This paper is structured in five parts. In Section 2, some background theory is presented. In Section 3 and Appendix A, we demonstrate that RNCRNs can approximate bifurcations of a given smooth dynamical system. In Section 4, we design RNCRNs that approximate piecewise systems, i.e. non-smooth systems that have different dynamical behaviours according to some externally imposed condition. Finally, in Section 5 and Appendix C, we demonstrate that RNCRNs can be used to construct dynamical behaviours entirely from relatively sparse data and demonstrate switching between dynamical regimes in this context.

2 Background

Chemical reaction networks (CRNs). A *chemical reaction network* (CRN) under mass-action kinetics is a set of chemical species which interact via a set of reactions whose speed is parametrized by rate coefficients [61]. This mathematical abstraction of chemistry is commonly used to model (bio)chemical systems in synthetic biology and DNA nanotechnology, including toggle switches in gene regulatory networks [62], chemotaxis in *E. coli* [63] and biological pattern formation [64].

For example, CRN



describes a single chemical species X_1 that is involved in degradation, auto-catalytic production and self-annihilation with the (dimensionless) rate coefficients respectively given by $\alpha_1, \alpha_2, \alpha_3 > 0$, and where \emptyset represents some chemical species that are of no interest. Under the assumption that chemical reactions occur in a well-mixed container, and that the chemical species are in high abundance, CRNs can be modelled deterministically with mass-action *reaction-rate equations* (RREs) - a system of ordinary-differential equations (ODEs) with polynomials on the right-hand side [61]. For example, CRN (1) has the corresponding RRE

$$\frac{dx_1}{dt} = (\alpha_2 - \alpha_1)x_1 - \alpha_3 x_1^2, \quad (2)$$

where $x_1 = x_1(t) \geq 0$ is the time-varying molecular concentration of the chemical species X_1 .

Recurrent neural chemical reaction networks (RNCRNs). In prior work, the authors have introduced a CRN based on artificial neural networks (ANNs), called the *recurrent neural chemical reaction network* (RNCRN) [51], and used it to approximate the dynamics of well-behaved ODE systems. In particular, given a target system of ODEs with suitably smooth right-hand side (vector field), given by

$$\frac{d\bar{x}_i}{dt} = f_i(\bar{x}_1, \dots, \bar{x}_n), \quad \bar{x}_i(0) \geq 0, \quad i = 1, 2, \dots, N, \quad (3)$$

there exists an RNCRN with the RREs

$$\begin{aligned} \frac{dx_i}{dt} &= \beta_i + x_i \sum_{j=1}^M \alpha_{i,j} y_j, & x_i(0) \geq 0, \quad i = 1, 2, \dots, N, \\ \frac{dy_j}{dt} &= \frac{\gamma}{\mu} + y_j \left(\sum_{i=1}^N \frac{\omega_{j,i}}{\mu} x_i + \frac{\theta_j}{\mu} \right) - \frac{1}{\mu} y_j^2, & y_j(0) \geq 0, \quad j = 1, 2, \dots, M, \end{aligned} \quad (4)$$

such that the concentration $x_i(t)$ approximates the target variable $\bar{x}_i(t)$ from (3) arbitrarily well. In particular, parameters $\beta_i, \gamma > 0$ from (4) are positive, while $\alpha_{i,j}, \omega_{j,i}, \theta_j \in \mathbb{R}$ can take any real value; furthermore, parameter $\mu > 0$ controls how fast the variables $y_j(t)$ are with respect to $x_i(t)$. For suitable values of these parameters, with $\mu > 0$ sufficiently small, i.e. with $y_j(t)$ sufficiently fast compared to $x_i(t)$, (4) approximates a given target system (3) arbitrarily well. In order to attempt to find such parameter values, Algorithm 1 is presented in [51].

The concentrations $x_i(t)$ and $y_j(t)$ respectively correspond to two sets of chemical species: the *executive* species X_i which manifest the target dynamical behaviour, and the *chemical perceptron* species Y_j which control the dynamics of the executive species through auxiliary reactions, which we illustrate in Figure 1. Chemical perceptrons Y_j are initially introduced in [56] and proposed as a chemical realisation of a feed-forward chemical neural network used for classification tasks, processing static input concentrations x_i to reach an equilibrium concentration y_j that corresponds to a classification decision. In the RNCRN, however, we introduce feedback reactions to the executive species X_i (see caption of Figure 1) that allow the output of a single layer of chemical perceptrons to dictate the dynamics of the executive species as they all evolve together.

The parameter $\mu > 0$ in (4) controls the time-scale separation between the fast perceptrons and the slow executive species. Due to the stability of the underlying chemical perceptrons [56], in the

formal limit $\mu \rightarrow 0$, the dynamics are governed by the *reduced* RNCRN with RREs

$$\frac{d\tilde{x}_i}{dt} = g_i(\tilde{x}_1, \dots, \tilde{x}_N) = \beta_i + \tilde{x}_i \sum_{j=1}^M \alpha_{i,j} \sigma_\gamma \left(\sum_{k=1}^N \omega_{j,k} \tilde{x}_k + \theta_j \right), \quad \tilde{x}(0) \geq 0, \quad i = 1, 2, \dots, N, \quad (5)$$

where σ_γ is a chemical activation function defined as $\sigma_\gamma(x) = (x + \sqrt{x^2 + 4\gamma})/2$. In this reduced limit, the chemical perceptrons operate as a conventional ANN with an activation function for each perceptron that approximates the commonly used ReLU activation function, allowing training of the RNCRN's parameters by standard methods. Loosely, Algorithm 1 in [51] uses standard machine learning methods to find an ANN such that $g_i(\tilde{x}_1, \dots, \tilde{x}_N) \approx f_i(\tilde{x}_1, \dots, \tilde{x}_N)$, and then relaxes the assumption that $\mu = 0$ to find a non-zero $\mu > 0$ such that the full RNCRN (4) approximates the target system (3) to a sufficient accuracy.

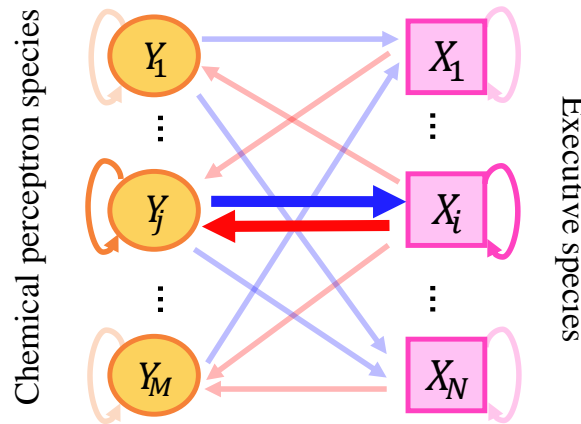


Figure 1: A graphical visualisation of the recurrent neural chemical reaction network (RNCRN) underlying the reaction-rate equations (RREs) (4), as introduced in [51]. Orange circles represent chemical perceptron species Y_1, \dots, Y_M , while magenta squares represent the executive species X_1, \dots, X_N . Coloured arrows represent chemical reactions consistent with the RREs: blue arrows represent $X_i + Y_j \xrightarrow{|\alpha_{i,j}|} 2X_i + Y_j$ or $X_i + Y_j \xrightarrow{|\alpha_{i,j}|} Y_j$ (according to the sign of $\alpha_{i,j}$), red arrows represent $X_i + Y_j \xrightarrow{|\omega_{j,i}|/\mu} X_i + 2Y_j$ or $X_i + Y_j \xrightarrow{|\omega_{j,i}|/\mu} X_i$ (according to the sign of $\omega_{j,i}$), magenta arrows represent $\emptyset \xrightarrow{\beta_i} X_i$, and orange arrows represent three reactions $\emptyset \xrightarrow{\gamma/\mu} Y_j$, $2Y_j \xrightarrow{1/\mu} Y_j$, and one of $Y_j \xrightarrow{|\theta_j|/\mu} 2Y_j$ or $Y_j \xrightarrow{|\theta_j|/\mu} \emptyset$ (according to the sign of θ_j).

Bifurcations. In (3), we have assumed that the target vector field $\mathbf{f} = (f_1, f_2, \dots, f_N)$ does not depend on any parameters. More broadly, we can relax this assumption by generalizing (3) to include a real parameter $\bar{\lambda}$, and consider the parameter-dependent target system

$$\frac{d\bar{x}_i}{dt} = f_i(\bar{x}_1, \dots, \bar{x}_n; \bar{\lambda}), \quad i = 1, 2, \dots, N, \quad (6)$$

where f_i depends on $\bar{\lambda}$ sufficiently smoothly. The value of $\bar{\lambda}$ can have a profound impact on the dynamical behaviour of (6). In particular, a *bifurcation* [4] is said to occur in (6) if, as $\bar{\lambda}$ is changed smoothly through a critical value $\bar{\lambda} = \bar{\lambda}^*$, the resulting long-time behaviour is qualitatively different below and above that critical value.

The example CRN (1) demonstrates that bifurcations are present even in relatively simple molecular systems. In particular, by writing the difference in rate coefficient as a single parameter

$\bar{\lambda} = (\alpha_2 - \alpha_1)$, and setting $\alpha_3 = 1$ such that the other coefficients are defined relative to α_3 , the associated RRE (2) is of the form (6). We observe that if $\bar{\lambda} > 0$ (i.e. $\alpha_2 > \alpha_1$), then molecular concentrations starting near zero, i.e. with $0 < x_1(0) \ll 1$, will equilibrate to $\bar{\lambda}$. However, if $\bar{\lambda} < 0$ (i.e. $\alpha_2 < \alpha_1$), then molecular concentrations starting near zero will equilibrate to zero. In the terminology of dynamical systems, the equilibrium $x_1^* = 0$ goes from stable to unstable as the parameter $\bar{\lambda}$ changes from negative to positive, while the other equilibrium $x_1^* = \lambda$ then goes from unstable to stable. This change of stability is an example of a bifurcation; in fact, ODE (2) is the normal form for *transcritical bifurcation* [4].

3 Bifurcations with parametrized RNCRNs

The RNCRN is introduced in [51] to approximate target systems of the form (3), with vector fields independent of parameters. In this section, we generalize the RNCRN to approximate parameter-dependent target systems. In particular, let us now consider as input data the target system

$$\begin{aligned} \frac{d\bar{x}_i}{dt} &= f_i(\bar{x}_1, \dots, \bar{x}_n, \bar{\lambda}_1, \dots, \bar{\lambda}_L), & \text{for } i = 1, 2, \dots, N, \\ \frac{d\bar{\lambda}_l}{dt} &= 0, & \text{for } l = 1, 2, \dots, L, \end{aligned} \quad (7)$$

whose vector field $\mathbf{f} = (f_1, f_2, \dots, f_N)$ depends sufficiently smoothly on L positive parameters $\bar{\lambda}_1, \bar{\lambda}_2, \dots, \bar{\lambda}_L > 0$, which can be seen as a generalization of (6); note that, if the parameters are not positive, then one can define new positive parameters by suitably shifting the old ones. In (7), we append the trivial ODEs for the parameters, allowing one to interpret them as auxiliary dependent variables. Provided that the initial conditions for these auxiliary variables match the target parameter values, the ODEs with parametrized vector fields, and those with vector fields depending on the auxiliary variables subject to trivial ODEs, are equivalent.

Parametrized RNCRNs. Let us now present a generalized RNCRN which can approximate the dynamics of the parameter-dependent target systems, represented in the form (7), over a range of parameter values. In particular, consider the *parametrized* RNCRN defined via the RREs

$$\begin{aligned} \frac{dx_i}{dt} &= \beta_i + x_i \sum_{j=1}^M \alpha_{i,j} y_j, & \text{for } i = 1, \dots, N, \\ \frac{d\lambda_l}{dt} &= 0, & \text{for } l = 1, \dots, L, \\ \frac{dy_j}{dt} &= \frac{\gamma_j}{\mu} + \left(\sum_{i=1}^N \frac{\omega_{j,i}}{\mu} x_i + \sum_{l=1}^L \frac{\psi_{j,l}}{\mu} \lambda_l + \frac{\theta_j}{\mu} \right) y_j - \frac{1}{\mu} y_j^2, & \text{for } j = 1, \dots, M, \end{aligned} \quad (8)$$

where $x_i = x_i(t) \geq 0$, $y_j = y_j(t) \geq 0$, $\lambda_l = \lambda_l(t) \geq 0$, $\beta_i, \gamma_j \geq 0$ and $\alpha_{i,j}, \omega_{j,i}, \theta_j, \psi_{j,l} \in \mathbb{R}$. In particular, compared to the original RNCRN (4), the parametrized RNCRN (8) contains additional executive species Λ_l , called *parameter-species*, which are static in the sense that they are governed by trivial ODEs $d\lambda_l/dt = 0$. Let us stress that, by representing parameters as species Λ_l in (8), their values are controlled via initial concentrations, as opposed to rate coefficients. Species Λ_l influence chemical perceptrons Y_j , but not vice-versa, and do so via the following catalytic reactions:

$$\Lambda_l + Y_j \xrightarrow{|\psi_{j,l}|/\mu} \Lambda_l + Y_j + \text{sign}(\psi_{j,l}) Y_j, \quad j = 1, 2, \dots, M, \quad l = 1, 2, \dots, L, \quad (9)$$

where, for brevity, $\text{sign}(\psi_{j,l})$ is used to indicate that the products contain two Y_j molecules when $\psi_{j,l}$ is positive, and none when it is negative. The parametrized RNCRN can be trained with a slight modification to Algorithm 1 from [51]; for completeness, we present this algorithm for (8) in Appendix D.1.

Since parameters can be represented as dependent variables with trivial dynamics, as in (8), one may expect that the RNCRN, which can approximate dependent variables undergoing dynamics resulting from arbitrary smooth vector fields [51], can also reproduce some bifurcations. In what follows, we numerically demonstrate via examples that the RNCRN can approximate two classical bifurcations, namely a Hopf bifurcation [4] and a homoclinic bifurcation [44, 65]. We note that both of these types of bifurcations have been observed in biochemical contexts [13, 14].

3.1 Hopf bifurcation

Let us apply RNCRNs to approximate the target system

$$\begin{aligned}\frac{d\bar{x}_1}{dt} &= (\bar{\lambda}_1 - 2 - (\bar{x}_1 - 5)^2 - (\bar{x}_2 - 5)^2)(\bar{x}_1 - 5) - (\bar{x}_2 - 5), \\ \frac{d\bar{x}_2}{dt} &= (\bar{\lambda}_1 - 2 - (\bar{x}_1 - 5)^2 - (\bar{x}_2 - 5)^2)(\bar{x}_2 - 5) + (\bar{x}_1 - 5), \\ \frac{d\bar{\lambda}_1}{dt} &= 0,\end{aligned}\tag{10}$$

which undergoes a Hopf bifurcation [4]. In particular, (10) is obtained from the normal form of a Hopf bifurcation by shifting the target equilibrium to $(\bar{x}_1, \bar{x}_2) = (5, 5)$, and the critical parameter value, at which the Hopf bifurcation occurs, to $\bar{\lambda}_1^* = 2$, so that the dynamics of interest are within the positive orthant. The (\bar{x}_1, \bar{x}_2) state-space of (10) is displayed in Figure 2(a) below, at and above the critical parameter value. In particular, when $\bar{\lambda}_1 = 1 < 2$, one can notice that the trajectories are attracted to the stable equilibrium $(\bar{x}_1, \bar{x}_2) = (5, 5)$, while for $\bar{\lambda}_1 = 3 > 2$ they are attracted to an isolated periodic orbit, called a limit cycle, enclosing the now unstable equilibrium $(\bar{x}_1, \bar{x}_2) = (5, 5)$.

One way to replicate this behaviour locally in the parameter space is to train the original RNCRN (4) to approximate (10) specifically at the bifurcation point $\bar{\lambda} = 1$. The results of such a training are presented in Appendix A.3, showing that the RNCRN numerically replicates the dynamics of (10) for parameter values in a small neighbourhood of $\bar{\lambda}_1^* = 2$. In particular, even though it is trained only at a single value $\bar{\lambda}_1^* = 2$, the RNCRN automatically reproduces the transition from stable equilibrium to stable limit cycle locally in the parameter space.

To replicate the dynamics of (10) over a larger set in the parameter space, we train the parametrized RNCRN of the form (8) to approximate (10) for all $1 \leq \bar{\lambda}_1 \leq 3$ with $M = 5$ chemical perceptrons; see Appendix A.1 for details. We display the state-space of the resulting RNCRN in Figure 2(b), demonstrating that qualitatively similar dynamics and bifurcation are inherited. Let us note that the RNCRN undergoes the Hopf bifurcation, not necessarily exactly at $\lambda_1 = 2$, but at a slightly different critical value, numerically found to be $\lambda_1 \approx 2.14$. This difference in the critical parameter values is a consequence of the approximating nature of the RNCRN, and can be reduced if the number and speed of chemical perceptrons is increased. However, in this paper, we focus on the RNCRNs with a smaller number of chemical perceptrons that still produce adequate behaviours, as CRNs with more species are, in general, more challenging to build experimentally.

3.2 Homoclinic bifurcation

Let us now consider the target system

$$\begin{aligned}\frac{d\bar{x}_1}{dt} &= \left(\bar{\lambda}_1 - 2 - \frac{4}{5}\right)(\bar{x}_1 - 5) + (\bar{x}_2 - 5) - \frac{6}{5}(\bar{x}_1 - 5)(\bar{x}_2 - 5) + \frac{3}{2}(\bar{x}_2 - 5)^2 \\ \frac{d\bar{x}_2}{dt} &= (\bar{x}_1 - 5) - \frac{4}{5}(\bar{x}_2 - 5) - \frac{4}{5}(\bar{x}_2 - 5)^2, \\ \frac{d\bar{\lambda}_1}{dt} &= 0,\end{aligned}\tag{11}$$

which undergoes a homoclinic bifurcation [44, 65] in the vicinity of the equilibrium $(\bar{x}_1, \bar{x}_2) = (5, 5)$ at the critical parameter value $\bar{\lambda}_1^* = 2$. The state-space of (11) is displayed in Figure 2(c) below, at and above the critical parameter value. In particular, when $\bar{\lambda}_1 = 1.9 < 2$, there is a stable limit cycles in the state-space, which is absent when $\bar{\lambda}_1 = 2.1 > 2$. This transition happens at $\bar{\lambda}_1 = 2$ via a homoclinic orbit - a solution in the state-space that connects the equilibrium $(\bar{x}_1, \bar{x}_2) = (5, 5)$ to itself. To replicate these dynamical behaviours, we train the parametrized RNCRN (8) with $M = 10$ chemical perceptron to approximate (10) for all $1.9 \leq \bar{\lambda}_1 \leq 2.1$; see Appendix A.2 for details. We show in Figure 2(d) that the RNCRN displays the desired dynamics.

Before closing this section, let us note that there are other systematic methods for designing CRNs with bifurcations [43, 44], such as Hopf or homoclinic bifurcations, which in general contain a smaller number of species and reactions compared to the RNCRNs. In particular, being based on ANNs, the strength of the RNCRNs is not necessarily in producing relatively small systems, but instead in being more versatile with the types of input data needed to achieve desired objectives. In the next two sections, we further explore this ability.

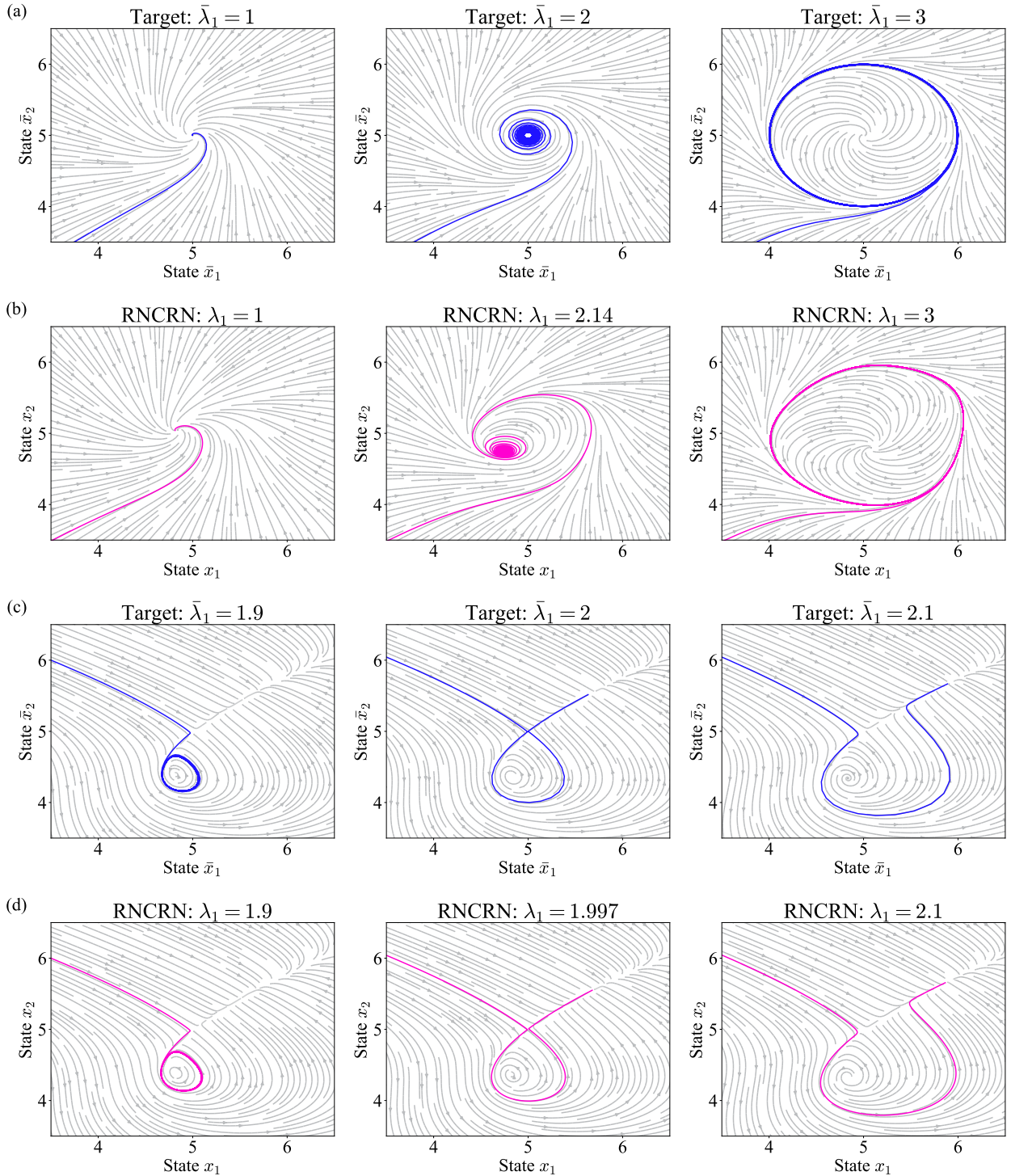


Figure 2: Approximation of two bifurcation-exhibiting ODEs using RNCRNs. Row (a) shows the target ODE (10) undergoing a Hopf bifurcation as the parameter $\bar{\lambda}_1$ is varied through its critical value. Row (b) shows the $M = 5$ chemical perceptron RNCRN approximation from Appendix A.1 with $\mu = 0.01$ undergoing the Hopf bifurcation as its equivalent control species λ_1 is varied. Row (c) shows the target ODE (11) undergoing a homoclinic bifurcation as the parameter $\bar{\lambda}_1$ is varied. Row (d) shows the $M = 10$ chemical perceptron RNCRN approximation from Appendix A.2 with $\mu = 0.0075$ undergoing a homoclinic bifurcation. The gray arrows show the vector field of the target ODEs for rows (a) and (b) while for rows (b) and (d) the arrows show the vector field of the reduced RNCRN (i.e. $\mu = 0$).

4 Piecewise systems with classification-controlled RNCNRNs

In Section 3, we have trained RNCNRNs to exhibit predefined bifurcations by using as input data the parametrized target ODEs of the form (7) which already display the desired bifurcations. Importantly, for classical bifurcations to exist in such ODEs, the vector field from (7) is required to be sufficiently smooth with respect to the parameters [66]. In this section, we relax this smoothness assumption by allowing the vector field from (7) to be discontinuous with respect to the parameters. The resulting ODEs are then known as *piecewise systems* [67], and provide more flexible training data for the RNCRN. In particular, on the one hand, this approach may allow one to simply specify suitable dynamics piecewise in the parameter space, thereby implicitly enforcing desired types of bifurcations at the associated boundaries, which the RNCRN is allowed to automatically interpolate. On the other hand, in some applications, more important may be that a system displays certain dynamical features for certain parameters values, rather than how it transitions between the different regimes, and the piecewise approach allows for this without imposing unnecessary regularity conditions on the dynamics. In what follows, we adapt the parametrized RNCRN from Section 3 to be trainable on such piecewise systems, replicating the desired dynamics for desired parameter values, while automatically connecting the different dynamical behaviours via suitable bifurcations.

4.1 Simple unstable-bistable piecewise system

As a motivation, let us consider the target system

$$\frac{d\bar{x}_1}{dt} = f_1(\bar{x}_1, \bar{\lambda}_1) = \begin{cases} 30 - 6\bar{x}_1, & \text{if } \bar{\lambda}_1 = 1, \\ -(\bar{x}_1 - 2)(\bar{x}_1 - 5)(\bar{x}_1 - 8), & \text{if } \bar{\lambda}_1 = 0. \end{cases} \quad (12)$$

In particular, the vector field has a unique stable equilibrium (unstability) when $\bar{\lambda}_1 = 1$, while it has two stable equilibria (bistability) when $\bar{\lambda}_1 = 0$. Being defined at only two isolated points in the parameter space, (12) is a piecewise system.

We train the parametrized RNCRN (8) with 3 chemical perceptrons to replicate the dynamics of (12), with details shown in Appendix B.1 and the training algorithm in Appendix D.2, and with the results presented in Figure 3. In particular, in Figure 3(a)–(d), we demonstrate that the RNCRN is unstable at $\lambda_1 = 1$ and bistable at $\lambda_1 = 0$, respectively, with the equilibria relatively close to those of (12).

As opposed to the target system (12), which is defined only at $\bar{\lambda}_1 = 1$ and $\bar{\lambda}_1 = 0$, the RNCRN is defined for all $\lambda_1 \geq 0$, and depends smoothly on this parameter. To analyse this dependence, we display in Figure 3(e) a bifurcation diagram - the equilibria of the RNCRN as a function of the parameter λ_1 . One can notice that the RNCRN automatically interpolates unstability at $\lambda_1 = 1$ and bistability at $\lambda_1 = 0$ via a classical bifurcation. In particular, one of the equilibria exists for all the parameter values shown in Figure 3(e), while the other two exist for all $\lambda_1 \in [0, \lambda_1^*)$ for some $\lambda_1^* < 10^{-2}$, after which they disappear via saddle-node bifurcation [4].

4.2 Classification-controlled RNCNRNs

Let us now consider a general target piecewise system taking the form

$$\frac{d\bar{x}_i}{dt} = f_i^{(p)}(\bar{x}_1, \dots, \bar{x}_N) \text{ for all } \bar{\lambda} \in \mathbb{L}_p, \quad i = 1, \dots, N, \quad p = 1, \dots, P, \quad (13)$$

where $\bar{\lambda} = (\bar{\lambda}_1, \bar{\lambda}_2, \dots, \bar{\lambda}_L) \in \mathbb{R}^L$ is the vector of parameters, $\mathbb{L}_1, \mathbb{L}_2, \dots, \mathbb{L}_P \subset \mathbb{R}^L$ are suitable disjoint sets in the parameter space, and $f_i^{(p)}$ is a suitably smooth function. In particular, when the

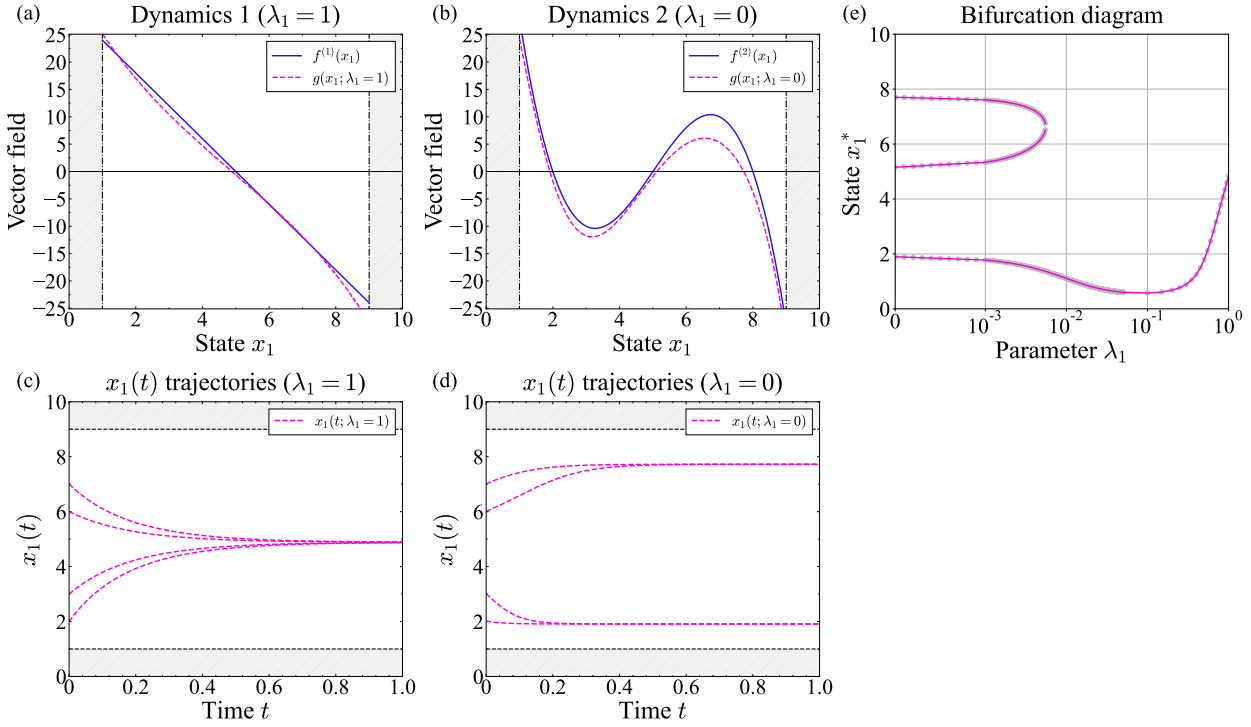


Figure 3: Emergence of a bifurcation via interpolation when an RNCRN is trained at discrete concentrations of a parameter species. Approximation of (12) by the parametrized RNCRN (33) specified in Appendix B.1. Panel (a) shows the dynamics in the first dynamical regime ($\lambda_1 = 1$). The target dynamics $d\bar{x}_1/dt = 30 - 6\bar{x}_1$ are shown in blue while the reduced vector field of the RNCRN approximation, i.e. when $\mu = 0$, are shown in magenta. Panel (b) shows the dynamics in the second dynamical regime ($\lambda_1 = 0$). In blue the target dynamics $d\bar{x}_1/dt = -(\bar{x}_1 - 2)(\bar{x}_1 - 5)(\bar{x}_1 - 8)$ while in magenta the reduced vector field of the RNCRN approximation. Panel (c)–(d) show $x_1(t)$ time-trajectories over a variety of executive species initial conditions, $x_1(0) = 2, 3, 6, 7$, for the full RNCRN in each dynamical regime with $\mu = 0.1$ and all chemical perceptron initial conditions at zero $y_1(0) = y_2(0) = y_3(0) = 0$. Panel (e) shows the bifurcation diagram for the RNCRN approximation as the parameter λ_1 is varied through intermediate values in magenta. A bifurcation is observed at around $\lambda_1 = 10^{-2}$.

parameters $\bar{\lambda}$ are chosen to lie in the set \mathbb{L}_p , the ODE is governed by the vector field $\mathbf{f}^{(p)}$. Let us note that set \mathbb{L}_p can be a single point. For example, system (12) is a special case of (13) with a single parameter $\bar{\lambda}_1$, and two single-point parameter regions $\mathbb{L}_1 = \{1\}$ and $\mathbb{L}_2 = \{0\}$.

The parametrized RNCRN (8) was sufficient to approximate piecewise system (12), which is defined at isolated parameter values. In order to approximate more general piecewise systems (13), which have more complicated parameter-space structure, we now modify the RNCRN. In particular, consider the parametrized RNCRN with RREs

$$\begin{aligned} \frac{dx_i}{dt} &= \beta_i + x_i \sum_{j=1}^M \alpha_{i,j} y_j, & i = 1, 2, \dots, N, \\ \frac{dy_j}{dt} &= \frac{\gamma_j}{\mu} + y_j \left(\sum_{i=1}^N \frac{\omega_{j,i}^{(y)}}{\mu} x_i + \frac{\theta_j^{(y)}}{\mu} + \frac{\psi_j}{\mu} r \right) - \frac{\tau_j}{\mu} y_j^2, & j = 1, 2, \dots, M, \end{aligned} \quad (14)$$

which are of the form (8) with a single parameter r , which itself is governed by the RREs

$$\begin{aligned} \frac{d\lambda_l}{dt} &= 0, & l &= 1, 2, \dots, L, \\ \frac{dz_k}{dt} &= \frac{\gamma}{\mu} + z_k \left(\sum_{l=1}^L \frac{\omega_{k,l}^{(z)}}{\mu} \lambda_l + \frac{\theta_k^{(z)}}{\mu} \right) - \frac{1}{\mu} z_k^2, & k &= 1, 2, \dots, K, \\ \frac{dr}{dt} &= \frac{\gamma}{\mu} + r \left(\sum_{k=1}^K \frac{\omega_k^{(r)}}{\mu} z_k + \frac{\theta_0^{(r)}}{\mu} \right) - \frac{1}{\mu} r^2, \end{aligned} \quad (15)$$

which involve auxiliary chemical perceptrons with concentrations z_1, z_2, \dots, z_K . We call the RNCRN corresponding to the RREs (14)–(15) the *classification-controlled* RNCRN, and illustrate it in Figure 4. Let us note that this RNCRN, like the original (4), contains only two time-scales: the slow species X_i and Λ_l , and the fast species Y_j, Z_k and R .

Loosely, (14) is designed to implement the dynamics of (13) point-wise, while (15) then assembles/classifies this dynamics to the appropriate parts of the parameter space. In particular, in the parametrized RNCRN (8), the ODEs for the chemical perceptron depend linearly on the parameters λ_l , while the perceptrons in (14) depend on λ_l only implicitly via the auxiliary variable r . Importantly, it follows from (15) that, for every sufficiently small $\mu > 0$,

$$z_k \approx \sigma_\gamma \left(\sum_{l=1}^L \omega_{k,l}^{(z)} \lambda_l(0) + \theta_k^{(z)} \right) \quad \text{and} \quad r \approx \sigma_\gamma \left(\sum_{k=1}^K \omega_k^{(r)} z_k + \theta_0^{(r)} \right), \quad (16)$$

where $\sigma_\gamma(x)$ is the activation function defined in (5). (16) therefore operates as a two-layer ANN, with a single perceptron in the second layer, that maps between parameters λ and the point-wise control parameter r .

Based on this modular design, we train the classification-controlled RNCRN in two steps. In the first step, we disregard the precise structure of the parameter space, and simply train the parametrized RNCRN (14) point-wise to display at some $r = r_p$ the dynamical behaviour induced by the vector field $\mathbf{f}^{(p)}$ for every $p = 1, 2, \dots, P$. Then, in the second step, we factor in the precise structure of the parameter space by training (15) to map from a given \mathbb{L}_p set in $(\lambda_1, \lambda_2, \dots, \lambda_L)$ -space to the associated r_p value by using standard feed-forward ANN training methods via (16). We present an algorithm for this training in Appendix D.3.

4.3 XOR-gated unistable-bistable piecewise system

Let us now consider a target piecewise system with more complicated parameter-space structure than (12), depending on two parameters $\bar{\lambda}_1, \bar{\lambda}_2$ and given by

$$\frac{d\bar{x}_1}{dt} = \begin{cases} 30 - 6\bar{x}_1, & \text{for all } (\bar{\lambda}_1, \bar{\lambda}_2) \in \mathbb{L}_1 = (\mathbb{K}_1 \times \mathbb{K}_2) \cup (\mathbb{K}_2 \times \mathbb{K}_1), \\ -(\bar{x}_1 - 2)(\bar{x}_1 - 5)(\bar{x}_1 - 8), & \text{for all } (\bar{\lambda}_1, \bar{\lambda}_2) \in \mathbb{L}_2 = (\mathbb{K}_1 \times \mathbb{K}_1) \cup (\mathbb{K}_2 \times \mathbb{K}_2), \end{cases} \quad (17)$$

where $\mathbb{K}_1 = [0, 1)$ and $\mathbb{K}_2 = [1, 2]$. Loosely, if on the domain $[0, 2] \times [0, 2]$ and one of the parameters is in the larger region, while the other is in the smaller region, then the piecewise system (17) is unistable; otherwise, it is bistable. This dependence can be interpreted as a XOR operator, and creates in the parameter space a non-linear boundary between different dynamical regions.

To approximate the dynamics of (17), we use Algorithm 4 to train the classification-controlled RNCRN (14)–(15), with details presented in Appendix B.2. In particular, in the first step of the

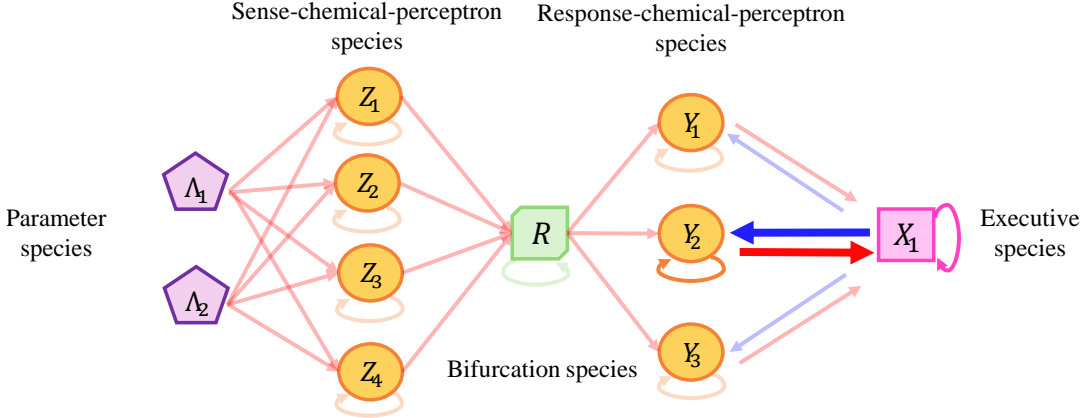


Figure 4: A schematic of the classification-controlled RNCRN used to approximate equation (17). In purple the parameter-species Λ_1 and Λ_2 are shown to interact with the sense-chemical-perceptron species that perform the non-linear classification presenting the output as the magnitude of the bifurcation species R . The bifurcation species R then acts as a parameter in the response-chemical-perceptron species that are trained to induce the intended dynamics in the executive species.

algorithm, we simply re-use the parametrized RNCRN from Appendix B.1, which was previously constructed in Section 4.1 to approximate system (12). In the second step, we then train the classification module (15) to implement the parameter-space structure from (17).

In Figure 5, we plot a two-parameter bifurcation diagram for the resulting RNCRN, displaying representative trajectories $x_1(t)$ at different points in the (λ_1, λ_2) parameter-space. One can notice a relatively good match with the target piecewise system (17): the RNCRN is unstable approximately when $(\lambda_1, \lambda_2) \in ([0, 1.0] \times [1.1, 2.0]) \cup ([1.1, 2.0] \times [0, 1.0])$, and bistable when $(\lambda_1, \lambda_2) \in ([0, 1.0] \times [0, 1.0]) \cup ([1.1, 2.0] \times [1.1, 2.0])$. Furthermore, the RNCRN depends smoothly on the parameters (λ_1, λ_2) , and interpolates the dynamics across the boundaries of the parameter space via saddle-node bifurcation (as shown in Figure 3 (e)).

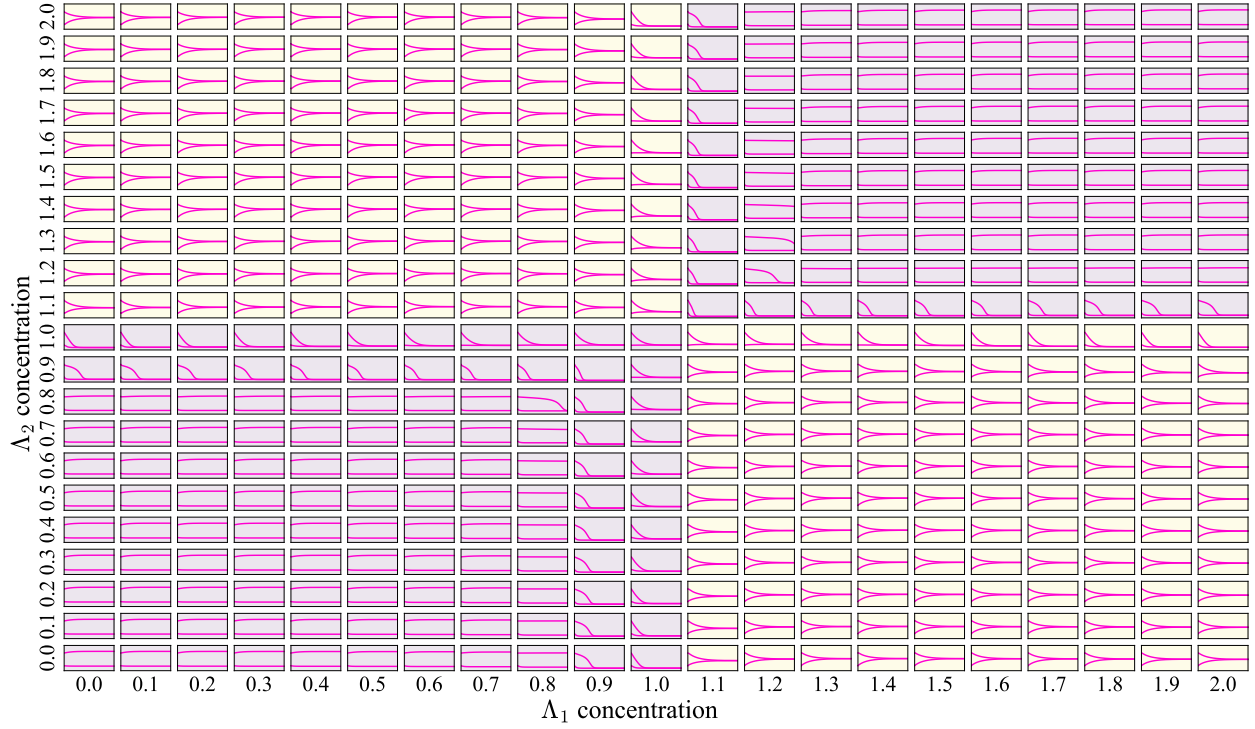


Figure 5: A panel of $x_1(t)$ trajectories for different concentrations of Λ_1 and Λ_2 showing the non-linear XOR classification boundary separating bistability and unistability for an RNCRN approximating the target piecewise system in equation (17). The associated classification-controlled RNCRN, i.e. equation (14), uses four sense chemical-perceptrons, one bifurcation chemical-perceptron, and three response chemical-perceptrons to induce the intended dynamics in one executive species according to the states of two parameter species Λ_1 and Λ_2 . Each panel has two time-trajectories simulated for a total time of $\Delta t = 1$ with $\mu = 0.001$, all chemical perceptron values starting at zero and the only executive species taking alternative values of $x_1(0) = 2$ and $x_1(0) = 7$. The hue of each panel shows the indented dynamical behaviour in the piecewise system: yellow should be unstable while pink should be bistable. Full details of the reactions in this example are given in Appendix B.2.

5 Data-defined limit cycles and switching

In both Sections 3 and 4, the RNCRNs are trained on the data taking the form of ODEs with suitably regular vector fields. In this section, we exploit the interpolation and extrapolation abilities of the underlying neural network-based methodology to show that the RNCRN can also be trained in an ODE-free manner from relatively sparse data: a set of points in the state-space. More precisely, we focus on generating the data that may allow the RNCRN to incorporate into its state-space two-dimensional limit cycles defined in an ODE-free manner.

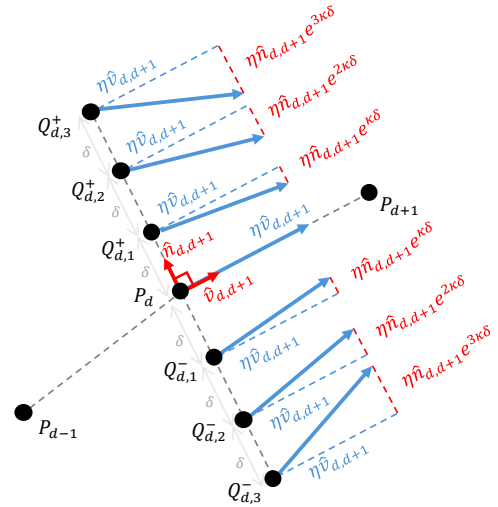
To this end, we sample a finite number of points on, and in a neighbourhood of, a given closed curve in the state-space. We then assign a single vector to each of these points with appropriate direction: the vectors on the closed curve point along it (corresponding to the limit cycle), while the remaining vectors all point either towards the closed curve or away from it (corresponding to respectively stability or instability). One thus obtains a local vector field, defined only on a finite number of states, which can be used to train the RNCRN, allowing it to extrapolate the behaviour beyond the grid. The algorithm to generate this data is given as Algorithm 1. Let us note that the vector field near the limit cycle varies exponentially with states in the algorithm; in Appendix C.3, we show that a linear variation can also be used. Let us also note that this algorithm can be generalized to higher dimensions; see Appendix C.6 for a three-dimensional version and an example.

Algorithm 1: *Algorithm for generating data to train RNCRNs to display two-dimensional stable limit cycles defined via the set of points $\{P_1, P_2, \dots, P_D, P_{D+1}\}$.*

Fix an ordered set of points in the executive-species space $\{P_1, P_2, \dots, P_D, P_{D+1}\}$, where $P_d \in \mathbb{R}_>^2$ for $d = 1, 2, \dots, D, D+1$ and such that $P_{D+1} = P_1$, where $\mathbb{R}_>^2$ is the positive quadrant. Fix also the padding number K , padding distance $\delta > 0$, decay scale $\kappa > 0$, and vector magnitude $\eta > 0$.

(a) **Padding points.** For each point P_d compute the unit normal vector $\hat{n}_{d,d+1}$ which is perpendicular to $\hat{v}_{d,d+1}$, the unit vector pointing from P_d to P_{d+1} . Create $2K$ symmetric padding points $Q_{d,k}^\pm = P_d \pm k\delta\hat{n}_{d,d+1}$ for $k = 1, 2, \dots, K$.

(b) **Local vector field.** Assign vector $\eta\hat{v}_{d,d+1}$ to P_d , and vector $(\eta\hat{v}_{d,d+1} \mp \eta\hat{n}_{d,d+1} \exp(\kappa\delta k))$ to $Q_{d,k}^\pm$.



5.1 Circular limit cycle

Consider a circle of radius $a > 0$ center at $(b_1, b_2) \in \mathbb{R}_>^2$, with parametric equation given by

$$\begin{aligned} x_1(s) &= a \cos(s) + b_1, \\ x_2(s) &= a \sin(s) + b_2, \end{aligned} \tag{18}$$

where $s \in [0, 2\pi)$. In what follows, we choose $a = 1$ and $(b_1, b_2) = (2, 2)$. We sample an ordered set of points $P_d = (x_1(s_d), x_2(s_d))$ by taking $s = s_d = 0.01(d - 1)$ in (18) for $d = 1, \dots, 629, 630$. Using Algorithm 1 with $K = 20$, $\delta = 0.01$, $\kappa = 1$, and $\eta = 1$, we generate the input data to train the RNCRN (4) with $M = 5$ chemical perceptrons to display in the state-space a stable two-dimensional limit cycle which is close to the circle. This training is performed by suitably adapting Algorithm 1 from [51], as presented in Algorithm 5 and Appendix C.1; see also Appendix C.2 for an example RNCRN with approximately circular limit cycle which is unstable.

We show the training data, together with the state-space of the trained RNCRN, in Figure 6(a). One can notice that the RNCRN with $\mu = 0.1$ numerically displays a stable limit cycle whose shape is relatively close to the desired circle. Furthermore, the RNCRN extends the vector consistently beyond this limit cycle, producing inside it an unstable equilibrium.

5.2 Heart-shaped limit cycle

Let us now consider the parametric equation

$$\begin{aligned} x_1(s) &= 2 + 1.12 \sin(s)^3, \\ x_2(s) &= 2 + 0.91 \cos(s) - 0.35 \cos(2s) - 0.14 \cos(3s) - 0.07 \cos(4s), \end{aligned} \quad (19)$$

which for $s \in [0, 2\pi)$ produces a heart shape in the (x_1, x_2) -space. In this example, we generate the training data for each lobe of the heart separately, $s_d = 0.01(d - 1)$ for $d = 1, 2, \dots, 261, 262$, and $d = 314, 315, \dots, 575, 576$, and then use Algorithm 1 with $K = 20$, $\delta = 0.01$, $\kappa = 1$, and $\eta = 1$; see Appendix C.4 for more details. We display the results in Figure 6(b), numerically demonstrating that the RNCRN displays a stable limit cycle that is approximately heart-shaped and, consistently with the given local vector field, creates an unstable equilibrium inside the cycle.

5.3 Multiple limit cycles

Algorithm 1 can also be used to train RNCRNs to display multiple coexisting limit cycles. For example, let us apply Algorithm 1 to generate data for two coexisting stable limit cycle of the form (18), one with $a = 0.5$ and $(b_1, b_2) = (1.5, 1.5)$, and the other with $a = 0.5$ and $(b_1, b_2) = (4.5, 1.5)$, as described in detail in Appendix C.5. The result of training an RNCRN on the concatenated training data is shown in Figure 6(c), numerically demonstrating two stable limit cycles. Let us note that, in this example, the RNCRN not only generates an unstable equilibrium inside each of the limit cycles, but also creates an equilibrium of saddle type as a way to connect the two regions specified by the training data.

5.4 Equilibrium-oscillation piecewise system with data-defined oscillations

Let us now combine the results from this section and Section 4, by considering the target piecewise system

$$\frac{d\mathbf{x}}{dt} = \begin{cases} \mathbf{f}^1(\mathbf{x}), & \text{for all } \bar{\lambda}_1 \in [0, 0.25], \\ \mathbf{f}^2(\mathbf{x}), & \text{for all } \bar{\lambda}_1 > 0.25, \end{cases} \quad (20)$$

with $\mathbf{x} \in \mathbb{R}^2$, where $\mathbf{f}^1(\mathbf{x}) \in \mathbb{R}^2$ is a smooth vector field with a unique stable equilibrium at $(0.5, 0.5)$, while $\mathbf{f}^2(\mathbf{x})$ is a vector field defined only on a finite number of states in $\mathbb{R}_>^2$ via Algorithm 1 to display a circular limit cycle. We might imagine chemical systems that implement dynamics such as (20) are implementing environment-specific oscillations. That is, when an environmental signal,

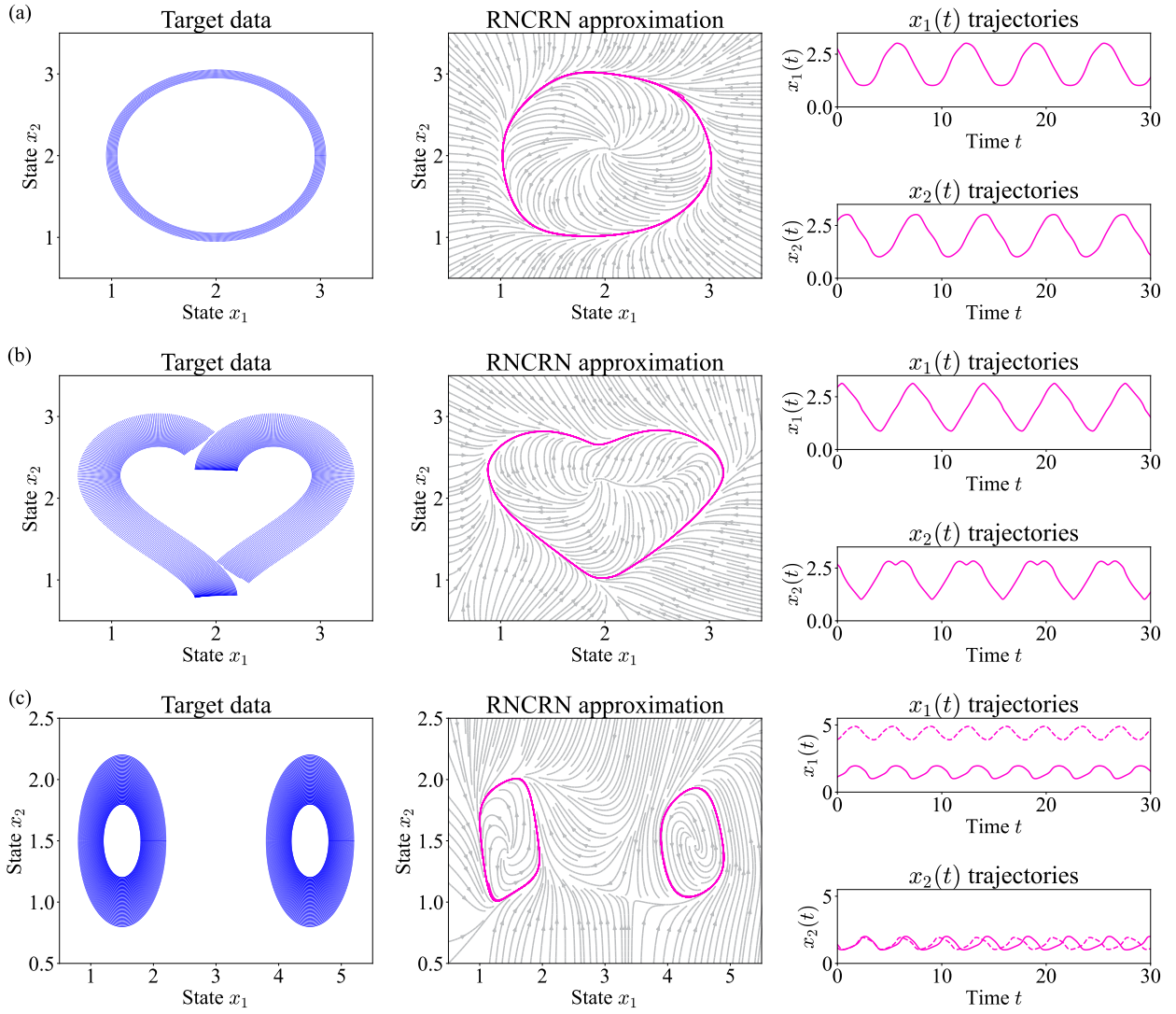


Figure 6: Example RNCRNs trained on data-defined limit cycles. Column 1 shows the points generated by Algorithm 1 at which the training data is given for different target attractor shapes. A close-up of the training data is shown in Appendix 1. Column 2 shows the RNCRN approximation trained on the data in column 1. The phase plane of the reduced RNCRN approximations, i.e. the RNCRN with $\mu = 0$, are shown as grey arrows, while example (x_1, x_2) -trajectories of the full RNCRNs with $\mu > 0$ are shown in magenta. Column 3 shows time-trajectories of the full RNCRN approximation. Row (a) shows a 5-chemical-perceptron RNCRN (full parameters are given in Appendix C.1) used to approximate a data-defined circular limit cycle. The time-trajectory was simulated with $x_1(0) = 2.744, x_2(0) = 2.693, \mu = 0.1$, and $y_1(0) = \dots, y_5(0) = 0$. Row (b) shows a 10-chemical-perceptron RNCRN (as specified in Appendix C.4) approximating the data-defined heart-shaped limit cycle. The time-trajectory was simulated with $x_1(0) = 2.957, x_2(0) = 2.665, \mu = 0.1$, and $y_1(0) = \dots, y_{10}(0) = 0$. Row (c) shows a 15-chemical-perceptron RNCRN (specified in Appendix C.5) approximating a system with two limit cycles. The two time-trajectories were both simulated with $\mu = 0.1$ and $y_1(0) = \dots, y_{15}(0) = 0$, the executive species' initial concentrations differed with $x_1(0) = 1.118, x_2(0) = 1.154$ or $x_1(0) = 3.916, x_2(0) = 1.392$.

Λ_1 , is abundant the system will produce oscillations of an executive species, X_1 , but when the environmental signal is weak, trace amounts of the executive species will be produced.

We now consider using a classification-controlled RNCRN, (14)–(15), to implement (20). Following the steps in Algorithm 4, modified as in Algorithm 5 to use the data-defined vector field, we train a classification-controlled RNCRN to implement (20); see Appendix C.7 for details (5 Y_j -chemical perceptrons, 3 Z_k -chemical perceptrons, and a single bifurcation species was used).

Figure 7(a)–(b) shows the data-defined oscillations and the stable equilibrium as blue arrows. The gray streamlines in Figure 7(a)–(b) shows the vector field of the reduced parametrized RNCRN for two particular values of the bifurcation species, $R = 0.1$ and $R = 1$, which were used in training. The input-output relationship between the parameter species Λ_1 and the bifurcation species R is shown in Figure 7(c).

To show the dependence of the X_1 behaviour on the parameter species Λ_1 , sub-panels in Figure 7(d) have been aligned with the λ_1^* -axis in Figure 7(c). Each sub-panel in Figure 7(d) corresponds to a different $\lambda_1(0)$ concentration and plots the resulting $x_1(t)$ time-trajectories. The full classification-controlled RNCRN is defined in Appendix C.7, and we simulate it using $\mu = 0.01$ and all chemical-perceptron species concentrations starting from zero. We observe that the classification-controlled RNCRN produces the desired behaviour. Below a critical value of $\lambda_1 \approx 2.5$ we observe that the $x_1(t)$ concentrations tends to a low equilibrium (the magenta panels in Figure 7(d)), but above that point we observe oscillations of a similar frequency and amplitude (the yellow panels in Figure 7(d)). This demonstrates an effective approximation of a piecewise systems as different regions of λ_1 -space are being mapping to different functions in (x_1, x_2) -space (and these functions are largely independent of λ_1 in these regions).

6 Discussion

In this work we use a recurrent neural chemical reaction network (RNCRN) architecture to approximate atypical dynamical behaviours and demonstrate that different dynamical regimes can be instantiated in a single system, along with bifurcations as the system moves between those regimes. Mapping target dynamical behaviours, in the form of a non-chemical target ODE, into a CRN has an extensive literature [31, 43–50]. These predominately analytical techniques can produce small CRNs in terms of reaction and species number. For example, the target ODE with a homoclinic bifurcation considered here (11) was realised with only 2 chemical species and 9 chemical reactions [44] compared to the 12 chemical species and 82 chemical reactions required by the RNCRN approximation identified here. Nonetheless, showing that RNCRNs can accurately replicate these bifurcations served as a motivation for the later sections where such analytical mapping techniques do not apply.

Sections 4 and 5 demonstrate the major advantage of the RNCRN over the aforementioned analytical techniques: RNCRNs are mathematically derived from artificial neural networks (ANNs) which are well-known for their ability to learn functions via data-driven training techniques. Exploiting this fact, we introduced Algorithm 1 for generating artificial data to train an RNCRN to reproduce isolated dynamical features defined on small regions of phase space. We were able to use Algorithm 1 to define exotic attractor shapes including a heart-shaped limit cycle, multiple limit cycles, and a three executive species toroidal limit cycle (see Appendix C.6).

A key feature of RNCRN-based methods was the ability of the RNCRN to extrapolate and interpolate dynamical behaviour to achieve dynamics in the whole space consistent with the features of interest. For example, we observe the presence of multiple equilibria that were not provided in the training data in the reduced vector fields of Figure 6. Similarly, bifurcations naturally emerge – without their location or type being specified explicitly – when RNCRNs are made to interpolate

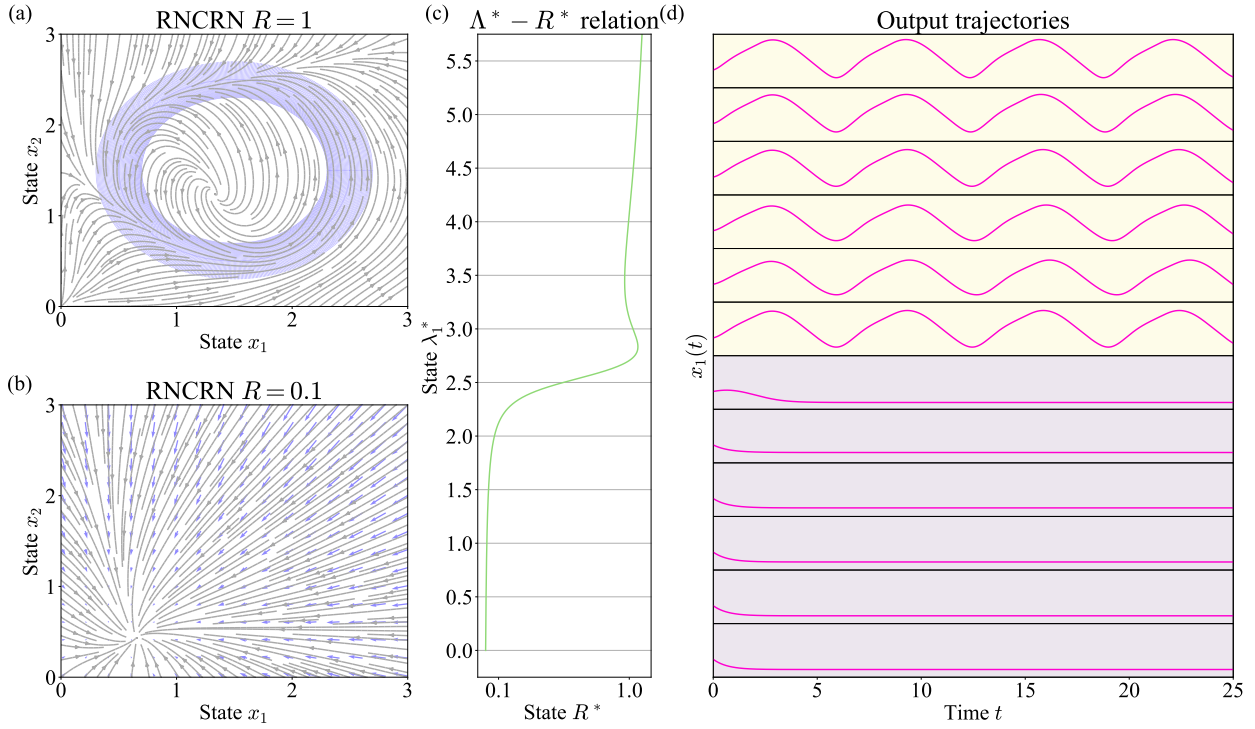


Figure 7: A classification-controlled RNCRN designed to approximate a piecewise system that either produces trace amounts of executive species X_1 or oscillations in X_1 according to the concentration of environmental species Λ_1 . Panel (a)–(b) shows the data-defined target dynamics (in blue) as well as the reduced vector field of the point-defined RNCRN approximation as grey arrows. Panel (c) shows the input-output relationship between Λ_1 and R (an intermediary species). Panel (d) shows numerically integrated time-trajectories of output species, $x_1(t)$, for the full RRE of the classification-controlled RNCRN with different $\lambda_1(0)$ values (according to the alignment with panel (c) λ_1^* -axis) and $\mu = 0.1$. Full details of the reactions in this system are given in Appendix C.7.

between qualitatively distinct behaviours at different values of the input parameters species. This ability for the RNCRN to fill in the gaps of the vector field makes it much easier to design complicated dynamics as there is no requirement to find an ODE with such dynamics.

In Section 5.4 we presented a classification-controlled RNCRN inspired by applications where it is necessary to sense the chemical environmental signals and act accordingly - in this case, turn on an oscillating output. Several major challenges with modern therapeutics could be addressed by systems with similar behaviour. Most straightforwardly, environmental-specific activation would allow for the localisation of therapeutic activity within pathologically relevant environments thus reducing off-target effects. It is well-known, for example, that off-target killing of benign cells limits the success of chemotherapies [68] and antibiotics therapies [69]. More interestingly for our purposes, switching to a new dynamical regime would allow fine-tuned control over the temporal concentration of a therapeutic species and would allow for the design of non-trivial dosing profiles. For example, it has been suggested that pulsatile dosing schedules are beneficial for preventing the development of resistance in a wide range of contexts including antibiotic resistance [70], cancer treatments [71], and preventing insulin resistance in diabetes treatments [72]. It should be noted that experimental chemical neural networks have already been built that are able to classify RNAs from cancer [73] and bacterial infections [23], highlighting that classification-controlled RNCRNs might one day be

developed in such contexts.

There are several outstanding challenges that remain to be explored in the context of RNCRNs. While the underlying reactions can, in principle, be encoded using DNA strand displacement [51], it is possible that other contexts such enzyme-aided DNA nanotechnology [74] or transcription factor networks [75] may be more convenient in practice. In that vein, the principles behind the construction of the RNCRN are more general than the particular CRNs used to instantiate the chemical perceptron. We anticipate that many alternative CRNs that play the equivalent role, *i.e.* weighted summation and non-linear activation, might be engineered to instantiate RNCRN-like systems in a range of biochemical media. We would like to explore systematic compilation methods that take the RNCRN’s chemical reaction network and converts them into a dynamically equivalent reaction network with alternative kinetic laws (such as enzyme-based synthetic biology).

An open question is whether interesting RNCRNs are feasible in practice. The number of reacting components in the RNCRNs presented in this work is lower than some other complex engineered molecular networks [21, 22], but a feature of RNCRNs that is more challenging to engineer is the necessary degree of connectivity between components and control over kinetics. We would therefore like to investigate compression or pruning algorithms to systematically reduce the number of auxiliary chemical species and chemical reactions within the resulting CRNs.

7 Declarations

Author Contributions: AD, TEO, and TP conceptualized the study; AD performed the simulations and wrote the original draft; TEO and TP reviewed and edited the final submission.

Funding: Alexander Dack acknowledges funding from the Department of Bioengineering at Imperial College London. Thomas E. Ouldridge would like to thank the Royal Society for a University Research Fellowship. Tomislav Plesa would like to thank Peterhouse, University of Cambridge, for a Fellowship.

Conflict of interest: The authors declare that they have no competing interests.

References

- [1] R. Lev Bar-Or, R. Maya, L. A. Segel, U. Alon, A. J. Levine, and M. Oren, “Generation of oscillations by the p53-Mdm2 feedback loop: A theoretical and experimental study,” *Proceedings of the National Academy of Sciences*, vol. 97, no. 21, pp. 11250–11255, 2000.
- [2] C. L. Manser and R. Perez-Carrasco, “A mathematical framework for measuring and tuning tempo in developmental gene regulatory networks,” *Development*, vol. 151, no. 12, p. dev202950, 2024.
- [3] J. Cerneckis, H. Cai, and Y. Shi, “Induced pluripotent stem cells (iPSCs): molecular mechanisms of induction and applications,” *Signal Transduction and Targeted Therapy*, vol. 9, no. 1, p. 112, 2024.
- [4] S. H. Strogatz, *Nonlinear Dynamics and Chaos*. CRC Press, 0 ed., 2018.
- [5] Y. Forterre, J. M. Skotheim, J. Dumais, and L. Mahadevan, “How the Venus flytrap snaps,” *Nature*, vol. 433, no. 7024, pp. 421–425, 2005.
- [6] G. F. Fussmann, S. P. Ellner, K. W. Shertzer, and N. G. Hairston Jr., “Crossing the Hopf Bifurcation in a Live Predator-Prey System,” *Science*, vol. 290, no. 5495, pp. 1358–1360, 2000.

- [7] R. M. Borisyuk and A. B. Kirillov, “Bifurcation analysis of a neural network model,” *Biological Cybernetics*, vol. 66, no. 4, pp. 319–325, 1992.
- [8] P. Érdi, T. Gröbler, G. Barna, and K. Kaski, “Dynamics of the olfactory bulb: bifurcations, learning, and memory,” *Biological Cybernetics*, vol. 69, no. 1, pp. 57–66, 1993.
- [9] E. M. Izhikevich, “Multiple cusp bifurcations,” *Neural Networks*, vol. 11, no. 3, pp. 495–508, 1998.
- [10] J. Ma and J. Wu, “Multistability and gluing bifurcation to butterflies in coupled networks with non-monotonic feedback,” *Nonlinearity*, vol. 22, no. 6, pp. 1383–1412, 2009.
- [11] L. Eisenmann, Z. Monfared, N. Göring, and D. Durstewitz, “Bifurcations and loss jumps in RNN training,” in *Advances in Neural Information Processing Systems* (A. Oh, T. Naumann, A. Globerson, K. Saenko, M. Hardt, and S. Levine, eds.), vol. 36, pp. 70511–70547, Curran Associates, Inc., 2023.
- [12] B. O. Palsson and T. M. Grotzans, “Mathematical modelling of dynamics and control in metabolic networks: VI. Dynamic bifurcations in single biochemical control loops,” *Journal of Theoretical Biology*, vol. 131, no. 1, pp. 43–53, 1988.
- [13] M. T. Borisuk and J. Tyson, “Bifurcation Analysis of a Model of Mitotic Control in Frog Eggs,” *Journal of Theoretical Biology*, vol. 195, pp. 69–85, Nov. 1998.
- [14] S. Kar, W. T. Baumann, M. R. Paul, and J. J. Tyson, “Exploring the roles of noise in the eukaryotic cell cycle,” *Proceedings of the National Academy of Sciences*, vol. 106, no. 16, pp. 6471–6476, 2009.
- [15] E. Marco, R. L. Karp, G. Guo, P. Robson, A. H. Hart, L. Trippa, and G.-C. Yuan, “Bifurcation analysis of single-cell gene expression data reveals epigenetic landscape,” *Proceedings of the National Academy of Sciences*, vol. 111, no. 52, 2014.
- [16] J. E. Ferrell, “Bistability, Bifurcations, and Waddington’s Epigenetic Landscape,” *Current Biology*, vol. 22, no. 11, pp. R458–R466, 2012.
- [17] L. Qian, E. Winfree, and J. Bruck, “Neural network computation with DNA strand displacement cascades,” *Nature*, vol. 475, pp. 368–372, 2011.
- [18] C. Kieffer, A. J. Genot, Y. Rondelez, and G. Gines, “Molecular Computation for Molecular Classification,” *Advanced Biology*, vol. 7, p. 2200203, 2023.
- [19] C. C. Samaniego, E. Wallace, F. Blanchini, E. Franco, and G. Giordano, “Neural networks built from enzymatic reactions can operate as linear and nonlinear classifiers,” *bioRxiv*, 2024.
- [20] A. J. Van Der Linden, P. A. Pieters, M. W. Bartelds, B. L. Nathalia, P. Yin, W. T. S. Huck, J. Kim, and T. F. A. De Greef, “DNA Input Classification by a Riboregulator-Based Cell-Free Perceptron,” *ACS Synthetic Biology*, vol. 11, pp. 1510–1520, 2022.
- [21] K. M. Cherry and L. Qian, “Scaling up molecular pattern recognition with DNA-based winner-take-all neural networks,” *Nature*, vol. 559, pp. 370–376, 2018.
- [22] X. Xiong, T. Zhu, Y. Zhu, M. Cao, J. Xiao, L. Li, F. Wang, C. Fan, and H. Pei, “Molecular convolutional neural networks with DNA regulatory circuits,” *Nature Machine Intelligence*, vol. 4, pp. 625–635, 2022.

[23] R. Lopez, R. Wang, and G. Seelig, “A molecular multi-gene classifier for disease diagnostics,” *Nature Chemistry*, vol. 10, no. 7, pp. 746–754, 2018.

[24] M. G. Baltussen, T. J. De Jong, Q. Duez, W. E. Robinson, and W. T. S. Huck, “Chemical reservoir computation in a self-organizing reaction network,” *Nature*, vol. 631, no. 8021, pp. 549–555, 2024.

[25] J. Stricker, S. Cookson, M. R. Bennett, W. H. Mather, L. S. Tsimring, and J. Hasty, “A fast, robust and tunable synthetic gene oscillator,” *Nature*, vol. 456, no. 7221, pp. 516–519, 2008.

[26] T. Fujii and Y. Rondelez, “Predator–Prey Molecular Ecosystems,” *ACS Nano*, vol. 7, no. 1, pp. 27–34, 2013.

[27] N. Srinivas, J. Parkin, G. Seelig, E. Winfree, and D. Soloveichik, “Enzyme-free nucleic acid dynamical systems,” *Science*, vol. 358, no. 6369, p. eaal2052, 2017.

[28] T. M. Bury, R. I. Sujith, I. Pavithran, M. Scheffer, T. M. Lenton, M. Anand, and C. T. Bauch, “Deep learning for early warning signals of tipping points,” *Proceedings of the National Academy of Sciences*, vol. 118, no. 39, p. e2106140118, 2021.

[29] S. Deb, S. Sidheekh, C. F. Clements, N. C. Krishnan, and P. S. Dutta, “Machine learning methods trained on simple models can predict critical transitions in complex natural systems,” *Royal Society Open Science*, vol. 9, no. 2, p. 211475, 2022.

[30] M. Demazure, “Catastrophe Theory,” in *Bifurcations and Catastrophes: Geometry of Solutions to Nonlinear Problems*, pp. 115–145, Berlin, Heidelberg: Springer Berlin Heidelberg, 2000.

[31] T. Plesa, A. Dack, and T. E. Ouldridge, “Integral feedback in synthetic biology: negative-equilibrium catastrophe,” *Journal of Mathematical Chemistry*, vol. 61, no. 9, pp. 1980–2018, 2023.

[32] G. Yang, D. Basanta, and G. Piliouras, “Bifurcation Mechanism Design—From Optimal Flat Taxes to Better Cancer Treatments,” *Games*, vol. 9, no. 2, p. 21, 2018.

[33] T. Yang, D. Hathcock, Y. Chen, P. L. McEuen, J. P. Sethna, I. Cohen, and I. Griniasty, “Bifurcation instructed design of multistate machines,” *Proceedings of the National Academy of Sciences*, vol. 120, no. 34, p. e2300081120, 2023.

[34] A. J. Genot, A. Baccouche, R. Sieskind, N. Aubert-Kato, N. Bredeche, J. F. Bartolo, V. Taly, T. Fujii, and Y. Rondelez, “High-resolution mapping of bifurcations in nonlinear biochemical circuits,” *Nature Chemistry*, vol. 8, no. 8, pp. 760–767, 2016.

[35] N. Lobato-Dauzier, A. Baccouche, G. Gines, T. Levi, Y. Rondelez, T. Fujii, S. H. Kim, N. Aubert-Kato, and A. J. Genot, “Neural coding of temperature with a DNA-based spiking chemical neuron,” *Nature Chemical Engineering*, vol. 1, no. 8, pp. 510–521, 2024.

[36] I. Otero-Muras and J. R. Banga, “Optimization-based prediction of fold bifurcations in nonlinear ODE models,” *IFAC-PapersOnLine*, vol. 51, no. 15, pp. 485–490, 2018.

[37] I. Otero-Muras, R. Perez-Carrasco, J. R. Banga, and C. P. Barnes, “Automated design of gene circuits with optimal mushroom-bifurcation behavior,” *iScience*, vol. 26, no. 6, p. 106836, 2023.

[38] G. Szep, N. Dalchau, and A. Csikász-Nagy, “Parameter Inference with Bifurcation Diagrams,” in *Advances in Neural Information Processing Systems* (M. Ranzato, A. Beygelzimer, Y. Dauphin, P. S. Liang, and J. W. Vaughan, eds.), vol. 34, pp. 5620–5630, Curran Associates, Inc., 2021.

[39] M. Fucho-Rius, S. Maretvadakethope, R. Pérez-Carrasco, A. Haro, T. Alarcón, and J. Sardanyés, “Local Nearby Bifurcations Lead to Synergies in Critical Slowing Down: the Case of Mushroom Bifurcations,” 2024.

[40] A. Mélot, E. Denimal, and L. Renson, “Multi-parametric optimization for controlling bifurcation structures,” *Proceedings of the Royal Society A: Mathematical, Physical and Engineering Sciences*, vol. 480, no. 2283, p. 20230505, 2024.

[41] I. Otero-Muras, P. Yordanov, and J. Stelling, “A method for inverse bifurcation of biochemical switches: inferring parameters from dose response curves,” *BMC Systems Biology*, vol. 8, no. 1, p. 114, 2014.

[42] M. Banaji, B. Boros, and J. Hofbauer, “Bifurcations in planar, quadratic mass-action networks with few reactions and low molecularity,” *Nonlinear Dynamics*, vol. 112, no. 23, pp. 21425–21448, 2024. arXiv: 2406.13451 [math].

[43] T. Plesa, T. Vejchodský, and R. Erban, “Chemical reaction systems with a homoclinic bifurcation: an inverse problem,” *Journal of Mathematical Chemistry*, vol. 54, no. 10, pp. 1884–1915, 2016.

[44] T. Plesa, “Mapping dynamical systems into chemical reactions,” 2024.

[45] E. H. Kerner, “Universal formats for nonlinear ordinary differential systems,” *Journal of Mathematical Physics*, vol. 22, no. 7, pp. 1366–1371, 1981.

[46] N. Samardzija, L. D. Greller, and E. Wasserman, “Nonlinear chemical kinetic schemes derived from mechanical and electrical dynamical systems,” *The Journal of Chemical Physics*, vol. 90, no. 4, pp. 2296–2304, 1989.

[47] K. Kowalski, “Universal formats for nonlinear dynamical systems,” *Chemical Physics Letters*, vol. 209, no. 1-2, pp. 167–170, 1993.

[48] D. Poland, “Cooperative catalysis and chemical chaos: a chemical model for the Lorenz equations,” *Physica D: Nonlinear Phenomena*, vol. 65, no. 1-2, pp. 86–99, 1993.

[49] K. M. Hangos and G. Szederkényi, “Mass action realizations of reaction kinetic system models on various time scales,” *Journal of Physics: Conference Series*, vol. 268, p. 012009, 2011.

[50] T. Plesa, T. Vejchodský, and R. Erban, “Test Models for Statistical Inference: Two-Dimensional Reaction Systems Displaying Limit Cycle Bifurcations and Bistability,” in *Stochastic Processes, Multiscale Modeling, and Numerical Methods for Computational Cellular Biology*, pp. 3–27, Springer International Publishing, 2017.

[51] A. Dack, B. Qureshi, T. E. Ouldridge, and T. Plesa, “Recurrent neural chemical reaction networks that approximate arbitrary dynamics,” 2025. arXiv:2406.03456.

[52] A. Hjelmfelt, E. D. Weinberger, and J. Ross, “Chemical implementation of neural networks and Turing machines.,” *Proceedings of the National Academy of Sciences*, vol. 88, pp. 10983–10987, 1991.

[53] J. Kim, J. Hopfield, and E. Winfree, “Neural Network Computation by In Vitro Transcriptional Circuits,” *Advances in Neural Information Processing Systems*, vol. 17, 2004.

[54] H.-J. K. Chiang, J.-H. R. Jiang, and F. Fages, “Reconfigurable neuromorphic computation in biochemical systems,” in *2015 37th Annual International Conference of the IEEE Engineering in Medicine and Biology Society (EMBC)*, pp. 937–940, 2015.

[55] W. Poole, A. Ortiz-Muñoz, A. Behera, N. S. Jones, T. E. Ouldridge, E. Winfree, and M. Gopalkrishnan, “Chemical Boltzmann Machines,” in *DNA 2017: DNA Computing and Molecular Programming*, vol. 10467, pp. 210–231, Springer International Publishing, 2017.

[56] D. F. Anderson, B. Joshi, and A. Deshpande, “On reaction network implementations of neural networks,” *Journal of The Royal Society Interface*, vol. 18, p. 20210031, 2021.

[57] J. Linder, Y.-J. Chen, D. Wong, G. Seelig, L. Ceze, and K. Strauss, “Robust Digital Molecular Design of Binarized Neural Networks,” in *27th International Conference on DNA Computing and Molecular Programming (DNA 27)*, vol. 205, pp. 1:1–1:20, 2021.

[58] R. T. Nagipogu and J. H. Reif, “NeuralCRNs: A Natural Implementation of Learning in Chemical Reaction Networks,” 2024.

[59] M. Vasić, C. Chalk, A. Luchsinger, S. Khurshid, and D. Soloveichik, “Programming and training rate-independent chemical reaction networks,” *Proceedings of the National Academy of Sciences*, vol. 119, p. e2111552119, 2022.

[60] A. Moorman, C. C. Samaniego, C. Maley, and R. Weiss, “A Dynamical Biomolecular Neural Network,” in *2019 IEEE 58th Conference on Decision and Control (CDC)*, pp. 1797–1802, 2019.

[61] M. Feinberg, “Lecture notes on Chemical Reaction Networks,” 1979.

[62] T. S. Gardner, C. R. Cantor, and J. J. Collins, “Construction of a genetic toggle switch in *Escherichia coli*,” *Nature*, vol. 403, no. 6767, pp. 339–342, 2000.

[63] T.-M. Yi, Y. Huang, M. I. Simon, and J. Doyle, “Robust perfect adaptation in bacterial chemotaxis through integral feedback control,” *Proceedings of the National Academy of Sciences*, vol. 97, no. 9, pp. 4649–4653, 2000.

[64] A. M. Turing, “The chemical basis of morphogenesis,” *Philosophical Transactions of the Royal Society of London. Series B, Biological Sciences*, vol. 237, no. 641, pp. 37–72, 1952.

[65] P. Glendinning, *Homoclinic Bifurcations in Ordinary Differential Equations*, pp. 285–293. Boston, MA: Springer US, 1987.

[66] L. Perko, *Differential Equations and Dynamical Systems*, vol. 7 of *Texts in Applied Mathematics*. New York, NY: Springer New York, 2001.

[67] A. F. Filippov, *Differential Equations with Discontinuous Righthand Sides*, vol. 18 of *Mathematics and Its Applications*. Dordrecht: Springer Netherlands, 1988.

[68] U. Anand, A. Dey, A. K. S. Chandel, R. Sanyal, A. Mishra, D. K. Pandey, V. De Falco, A. Upadhyay, R. Kandimalla, A. Chaudhary, J. K. Dhanjal, S. Dewanjee, J. Vallamkondu, and J. M. Pérez De La Lastra, “Cancer chemotherapy and beyond: Current status, drug candidates, associated risks and progress in targeted therapeutics,” *Genes & Diseases*, vol. 10, no. 4, pp. 1367–1401, 2023.

[69] D. V. Patangia, C. Anthony Ryan, E. Dempsey, R. Paul Ross, and C. Stanton, “Impact of antibiotics on the human microbiome and consequences for host health,” *MicrobiologyOpen*, vol. 11, no. 1, p. e1260, 2022.

[70] C. M. Baker, M. J. Ferrari, and K. Shea, “Beyond dose: Pulsed antibiotic treatment schedules can maintain individual benefit while reducing resistance,” *Scientific Reports*, vol. 8, no. 1, p. 5866, 2018.

[71] X. Wang, H. Zhang, and X. Chen, “Drug resistance and combating drug resistance in cancer,” *Cancer Drug Resistance*, 2019.

[72] L. S. Satin, P. C. Butler, J. Ha, and A. S. Sherman, “Pulsatile insulin secretion, impaired glucose tolerance and type 2 diabetes,” *Molecular Aspects of Medicine*, vol. 42, pp. 61–77, 2015.

[73] C. Zhang, Y. Zhao, X. Xu, R. Xu, H. Li, X. Teng, Y. Du, Y. Miao, H.-c. Lin, and D. Han, “Cancer diagnosis with DNA molecular computation,” *Nature Nanotechnology*, vol. 15, no. 8, pp. 709–715, 2020.

[74] S. Shah, T. Song, X. Song, M. Yang, and J. Reif, “Implementing Arbitrary CRNs Using Strand Displacing Polymerase,” in *DNA Computing and Molecular Programming* (C. Thachuk and Y. Liu, eds.), vol. 11648, pp. 21–36, Cham: Springer International Publishing, 2019.

[75] R. Zhu, J. M. Del Rio-Salgado, J. Garcia-Ojalvo, and M. B. Elowitz, “Synthetic multistability in mammalian cells,” *Science*, vol. 375, no. 6578, p. eabg9765, 2022.

[76] D. E. Rumelhart, G. E. Hinton, and R. J. Williams, “Learning representations by back-propagating errors,” *Nature*, vol. 323, no. 6088, pp. 533–536, 1986.

[77] A. Dack, T. Plesa, and T. E. Ouldridge, “github.com/alexdack/rncrn_bifs_data_def_piecewise,” Jul 2026.

[78] J. Bradbury, R. Frostig, P. Hawkins, M. J. Johnson, C. Leary, D. Maclaurin, G. Necula, A. Paszke, J. VanderPlas, S. Wanderman-Milne, and Q. Zhang, “JAX: composable transformations of Python+NumPy programs,” 2026. original-date: 2018-10-25T21:25:02Z.

[79] DeepMind, I. Babuschkin, K. Baumli, A. Bell, S. Bhupatiraju, J. Bruce, P. Buchlovsky, D. Budden, T. Cai, A. Clark, I. Danihelka, A. Dedieu, C. Fantacci, J. Godwin, C. Jones, R. Hemsley, T. Hennigan, M. Hessel, S. Hou, S. Kapturowski, T. Keck, I. Kemaev, M. King, M. Kunesch, L. Martens, H. Merzic, V. Mikulik, T. Norman, G. Papamakarios, J. Quan, R. Ring, F. Ruiz, A. Sanchez, L. Sartran, R. Schneider, E. Sezener, S. Spencer, S. Srinivasan, M. Stanojević, W. Stokowiec, L. Wang, G. Zhou, and F. Viola, “The DeepMind JAX Ecosystem,” 2020.

A Appendix: Example bifurcations

A.1 Hopf bifurcation

We use Algorithm 2, a modified version of Algorithm 1 from [51] with static executive species, to approximate the target system (10) on $\mathbb{K}_1 = [3.5, 6.5]$, $\mathbb{K}_2 = [3.5, 6.5]$ and $\mathbb{L} = [1, 3]$ with a parametrized RNCRN. The absolute tolerance $\varepsilon \approx 10^{-1}$ is met with an RNCRN with $M = 5$ chemical perceptrons and coefficients $\beta_1 = \beta_2 = 260$, $\gamma = 1$, and

$$\boldsymbol{\alpha}_1 = \begin{pmatrix} -4.315 \\ -5.861 \\ -9.788 \\ 3.796 \\ -1.209 \end{pmatrix}, \quad \boldsymbol{\alpha}_2 = \begin{pmatrix} -1.505 \\ -4.968 \\ 0.149 \\ -25.501 \\ 0.824 \end{pmatrix}, \quad \boldsymbol{\theta} = \begin{pmatrix} 10.656 \\ 8.520 \\ 5.385 \\ 3.369 \\ 4.653 \end{pmatrix},$$

$$\boldsymbol{\omega}_1 = \begin{pmatrix} -1.298 \\ -0.228 \\ -1.545 \\ 0.103 \\ -2.239 \end{pmatrix}, \quad \boldsymbol{\omega}_2 = \begin{pmatrix} -0.599 \\ -0.131 \\ 0.061 \\ -0.940 \\ 1.676 \end{pmatrix}, \quad \boldsymbol{\psi} = \begin{pmatrix} 0.105 \\ -0.080 \\ 0.070 \\ 0.039 \\ 0.069 \end{pmatrix}, \quad (21)$$

where $\boldsymbol{\alpha}_i = (\alpha_{i,1}, \alpha_{i,2}, \dots, \alpha_{i,5})^\top$ for $i = 1, 2$, $\boldsymbol{\omega}_i = (\omega_{1,i}, \omega_{2,i}, \dots, \omega_{5,i})^\top$ for $i = 1, 2$, $\boldsymbol{\theta} = (\theta_1, \theta_2, \dots, \theta_5)^\top$, and $\boldsymbol{\psi} = (\psi_1, \psi_2, \dots, \psi_5)^\top$. The reduced ODEs are given by

$$\frac{d\tilde{x}_1}{dt} = g_1(\tilde{x}_1, \tilde{x}_2; \lambda_1) = 260 + \tilde{x}_1 \sum_{j=1}^5 \alpha_{1,j} \sigma_1(\omega_{j,1} \tilde{x}_1 + \omega_{j,2} \tilde{x}_2 + \psi_j \lambda_1 + \theta_j),$$

$$\frac{d\tilde{x}_2}{dt} = g_2(\tilde{x}_1, \tilde{x}_2; \lambda_1) = 260 + \tilde{x}_2 \sum_{j=1}^5 \alpha_{2,j} \sigma_1(\omega_{j,1} \tilde{x}_1 + \omega_{j,2} \tilde{x}_2 + \psi_j \lambda_1 + \theta_j), \quad (22)$$

while the full ODEs read

$$\frac{dx_1}{dt} = 260 + x_1 \left(\sum_{j=1}^5 \alpha_{1,j} y_j \right), \quad \frac{dx_2}{dt} = 260 + x_2 \left(\sum_{j=1}^5 \alpha_{2,j} y_j \right),$$

$$\mu \frac{dy_1}{dt} = 1 + \left(\sum_{i=1}^2 \omega_{1,i} x_i + \psi_1 \lambda_1 + \theta_1 \right) y_1 - y_1^2, \quad \mu \frac{dy_2}{dt} = 1 + \left(\sum_{i=1}^2 \omega_{2,i} x_i + \psi_2 \lambda_1 + \theta_2 \right) y_2 - y_2^2,$$

$$\mu \frac{dy_3}{dt} = 1 + \left(\sum_{i=1}^2 \omega_{3,i} x_i + \psi_3 \lambda_1 + \theta_3 \right) y_3 - y_3^2, \quad \mu \frac{dy_4}{dt} = 1 + \left(\sum_{i=1}^2 \omega_{4,i} x_i + \psi_4 \lambda_1 + \theta_4 \right) y_4 - y_4^2,$$

$$\mu \frac{dy_5}{dt} = 1 + \left(\sum_{i=1}^2 \omega_{5,i} x_i + \psi_5 \lambda_1 + \theta_5 \right) y_5 - y_5^2, \quad \frac{d\lambda_1}{dt} = 0, \quad (23)$$

Here, we assume general initial concentrations: $x_1(0) = a_1 \in [3.5, 6.5]$, $x_2(0) = a_2 \in [3.5, 6.5]$, and $y_1(0) = b_1 \geq 0$, $y_2(0) = b_2 \geq 0$, $y_3(0) = b_3 \geq 0$, $y_4(0) = b_4 \geq 0$, and $y_5(0) = b_5 \geq 0$. The coefficients were rounded to 3 decimal places to quote in the text, the full precision coefficients are available in the code repository.

In Figure 2, we used a range of initial conditions for the executive species, but the chemical perceptron species always started at zero. For Figure 2 (a) we used $\bar{x}_1(0) = 2$, $\bar{x}_2(0) = 2$, and for the RNCRN approximation in Figure 2 (b) we used $x_1(0) = 2$, $x_2(0) = 2$.

A.2 Homoclinic bifurcation

We use Algorithm 2, a modified version of Algorithm 1 from [51] with static executive species, to approximate the target system (11) on $\mathbb{K}_1 = [3.5, 6.5]$, $\mathbb{K}_2 = [3.5, 6.5]$ and $\mathbb{L} = [1.9, 2.1]$ with a parametrized RNCRN. Tolerance $\varepsilon \approx 10^{-3}$ is met with an RNCRN with $M = 10$ chemical perceptrons and coefficients $\beta_1 = \beta_2 = 1$, $\gamma = 1$, and

$$\boldsymbol{\alpha}_1 = \begin{pmatrix} 0.307 \\ -0.533 \\ 0.324 \\ 0.999 \\ 4.348 \\ 1.820 \\ -2.823 \\ -0.744 \\ -1.270 \\ 0.837 \end{pmatrix}, \quad \boldsymbol{\alpha}_2 = \begin{pmatrix} 0.812 \\ 0.923 \\ -0.425 \\ -0.260 \\ -0.191 \\ -2.821 \\ -0.174 \\ 0.228 \\ -0.349 \\ -0.636 \end{pmatrix}, \quad \boldsymbol{\theta} = \begin{pmatrix} 0.790 \\ 1.455 \\ -1.391 \\ 3.440 \\ -1.901 \\ 3.461 \\ 0.657 \\ 0.634 \\ 1.932 \\ -3.335 \end{pmatrix},$$

$$\boldsymbol{\omega}_1 = \begin{pmatrix} 0.372 \\ -0.183 \\ -0.205 \\ 0.448 \\ -0.986 \\ -0.056 \\ -0.763 \\ 1.043 \\ -0.253 \\ 0.271 \end{pmatrix}, \quad \boldsymbol{\omega}_2 = \begin{pmatrix} -0.697 \\ 0.084 \\ 0.835 \\ -1.034 \\ 0.797 \\ -1.153 \\ 0.025 \\ -0.515 \\ -0.296 \\ 0.335 \end{pmatrix}, \quad \boldsymbol{\psi} = \begin{pmatrix} 0.364 \\ -0.022 \\ -0.781 \\ -0.085 \\ 0.062 \\ -0.023 \\ 0.586 \\ -0.556 \\ 0.323 \\ 0.385 \end{pmatrix}, \quad (24)$$

where $\boldsymbol{\alpha}_i = (\alpha_{i,1}, \alpha_{i,2}, \dots, \alpha_{i,10})^\top$ for $i = 1, 2$, $\boldsymbol{\omega}_i = (\omega_{1,i}, \omega_{2,i}, \dots, \omega_{10,i})^\top$ for $i = 1, 2$, $\boldsymbol{\theta} = (\theta_1, \theta_2, \dots, \theta_{10})^\top$, and $\boldsymbol{\psi} = (\psi_1, \psi_2, \dots, \psi_{10})^\top$. The reduced ODEs are given by

$$\begin{aligned} \frac{d\tilde{x}_1}{dt} &= g_1(\tilde{x}_1, \tilde{x}_2; \lambda_1) = 1 + \tilde{x}_1 \sum_{j=1}^{10} \alpha_{1,j} \sigma_1(\omega_{j,1} \tilde{x}_1 + \omega_{j,2} \tilde{x}_2 + \psi_j \lambda_1 + \theta_j), \\ \frac{d\tilde{x}_2}{dt} &= g_2(\tilde{x}_1, \tilde{x}_2; \lambda_1) = 1 + \tilde{x}_2 \sum_{j=1}^{10} \alpha_{2,j} \sigma_1(\omega_{j,1} \tilde{x}_1 + \omega_{j,2} \tilde{x}_2 + \psi_j \lambda_1 + \theta_j), \end{aligned} \quad (25)$$

while the full ODEs read

$$\begin{aligned}
\frac{dx_1}{dt} &= 1 + x_1 \left(\sum_{j=1}^{10} \alpha_{1,j} y_j \right), & \frac{dx_2}{dt} &= 1 + x_2 \left(\sum_{j=1}^{10} \alpha_{2,j} y_j \right), \\
\mu \frac{dy_1}{dt} &= 1 + \left(\sum_{i=1}^2 \omega_{1,i} x_i + \psi_1 \lambda_1 + \theta_1 \right) y_1 - y_1^2, & \mu \frac{dy_2}{dt} &= 1 + \left(\sum_{i=1}^2 \omega_{2,i} x_i + \psi_2 \lambda_1 + \theta_2 \right) y_2 - y_2^2, \\
\mu \frac{dy_3}{dt} &= 1 + \left(\sum_{i=1}^2 \omega_{3,i} x_i + \psi_3 \lambda_1 + \theta_3 \right) y_3 - y_3^2, & \mu \frac{dy_4}{dt} &= 1 + \left(\sum_{i=1}^2 \omega_{4,i} x_i + \psi_4 \lambda_1 + \theta_4 \right) y_4 - y_4^2, \\
\mu \frac{dy_5}{dt} &= 1 + \left(\sum_{i=1}^2 \omega_{5,i} x_i + \psi_5 \lambda_1 + \theta_5 \right) y_5 - y_5^2, & \mu \frac{dy_6}{dt} &= 1 + \left(\sum_{i=1}^2 \omega_{6,i} x_i + \psi_6 \lambda_1 + \theta_6 \right) y_6 - y_6^2, \\
\mu \frac{dy_7}{dt} &= 1 + \left(\sum_{i=1}^2 \omega_{7,i} x_i + \psi_7 \lambda_1 + \theta_7 \right) y_7 - y_7^2, & \mu \frac{dy_8}{dt} &= 1 + \left(\sum_{i=1}^2 \omega_{8,i} x_i + \psi_8 \lambda_1 + \theta_8 \right) y_8 - y_8^2, \\
\mu \frac{dy_9}{dt} &= 1 + \left(\sum_{i=1}^2 \omega_{9,i} x_i + \psi_9 \lambda_1 + \theta_9 \right) y_9 - y_9^2, & \mu \frac{dy_{10}}{dt} &= 1 + \left(\sum_{i=1}^2 \omega_{10,i} x_i + \psi_{10} \lambda_1 + \theta_{10} \right) y_{10} - y_{10}^2, \\
\frac{d\lambda_1}{dt} &= 0
\end{aligned} \tag{26}$$

Here, we assume general initial concentrations: $x_1(0) = a_1 \in [3, 7]$, $x_2(0) = a_2 \in [3, 7]$, and $y_1(0) = b_1 \geq 0$, $y_2(0) = b_2 \geq 0$, $y_3(0) = b_3 \geq 0$, $y_4(0) = b_4 \geq 0$, $y_5(0) = b_5 \geq 0$, $y_6(0) = b_6 \geq 0$, $y_7(0) = b_7 \geq 0$, $y_8(0) = b_8 \geq 0$, $y_9(0) = b_9 \geq 0$, and $y_{10}(0) = b_{10} \geq 0$. The coefficients were rounded to 3 decimal places to quote in the text, the full precision coefficients are available in the code repository. A lower absolute tolerance was required in this example as the homoclinic orbit is a delicate dynamical behaviour to approximate effectively.

In Figure 2, we used a range of initial conditions for the executive species, but the chemical perceptron species always started at zero. For the homoclinic bifurcation we used slightly different executive species concentrations due to the sensitivity of the homoclinic orbit. In Figure 2 (c) we used: $\bar{x}_1(0) = 3.5$, $\bar{x}_2(0) = 6.0$ for the sub-panel with $\bar{\lambda}_1 = 1.9$; and $\bar{x}_1(0) = 3.5$, $\bar{x}_2(0) = 6.0435$ for the sub-panel with $\bar{\lambda}_1 = 2$ and $\bar{\lambda}_1 = 2.1$. In Figure 2 (d) we used: $x_1(0) = 3.5$, $x_2(0) = 6.0$ for the sub-panel with $\lambda_1 = 1.9$; $x_1(0) = 3.5$, $x_2(0) = 6.04$ for the sub-panel with $\lambda_1 = 1.997$; and $x_1(0) = 3.5$, $x_2(0) = 6.0435$ for the sub-panel with $\lambda_1 = 2.1$.

A.3 Hopf bifurcation by training at criticality alone

We now demonstrate that by training a RNCRN at the critical point of a Hopf bifurcation it is possible to find random perturbation of the RNCRN's parameters that recreate the qualitative behaviour of a Hopf bifurcation without any data about either side of the bifurcation being used during training.

Consider the target ODE for a Hopf bifurcation at its critical point with an equilibrium at $(x_1, x_2) = (5, 5)$

$$\begin{aligned}
\frac{d\bar{x}_1}{dt} &= (-(\bar{x}_1 - 5)^2 - (\bar{x}_2 - 5)^2)(\bar{x}_1 - 5) - (\bar{x}_2 - 5), \\
\frac{d\bar{x}_2}{dt} &= (-(\bar{x}_1 - 5)^2 - (\bar{x}_2 - 5)^2)(\bar{x}_2 - 5) + (\bar{x}_1 - 5).
\end{aligned} \tag{27}$$

In Figure 2(a) the $\bar{\lambda} = 2$ plot visualises the dynamics of (27). We train an RNCRN to approximate (27) and show the associated vector field of the reduced RNCRN and an example $(x_1(t), x_2(t))$ trajectory

in Figure 8(b). In Figures 8(a) and (c) we show that by inducing a particular but randomly sampled perturbation of the rate constants we can induce unstable or oscillatory behaviour. Unlike the parametrized RNCRN the training of an RNCRN at criticality alone does not use data about bifurcation parameter, instead this behaviour emerges, showing that the RNCRN is reproducing key features of the mathematical structure of the underlying ODE (27).

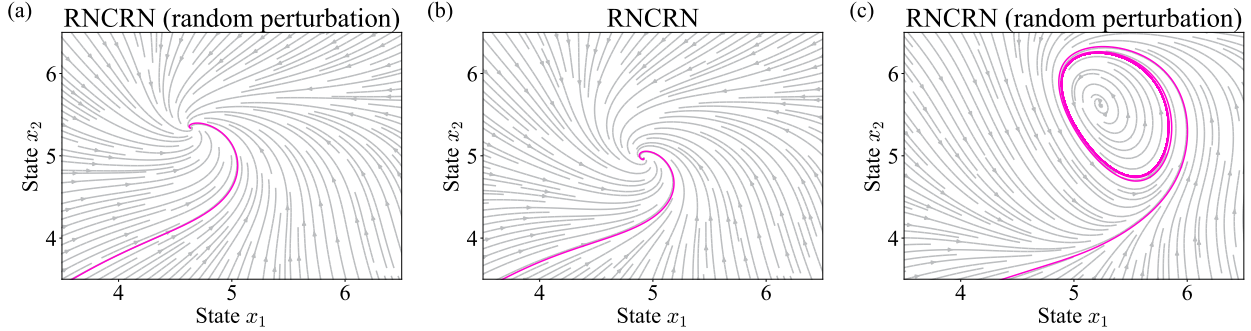


Figure 8: An RNCRN trained at the critical point of a Hopf bifurcation, i.e. (27), demonstrating extrapolation of dynamics to behaviours outside of the training data. Panel (b) shows the $M = 6$ chemical perceptron RNCRN trained to approximate (27) while panels (a) and (c) show the same RNCRN approximation with the rates randomly perturbed (see Appendix A.3 for the rates of the RNCRNs). All panels show their respective reduced RNCRN vector field as grey arrows and a $(x_1(t), x_2(t))$ -time-trajectories with $\mu = 0.01$, and initial concentrations $x_1(0) = x_2(0) = 2$ and $y_1(0) = \dots = y_6(0) = 0$ in magenta.

We use Algorithm 1 from [51] to approximate the target system (27) on $\mathbb{K}_1 = [3.5, 6.5], \mathbb{K}_2 = [3.5, 6.5]$ with a single-layer RNCRN (not parameterized). Tolerance $\varepsilon \approx 10^0$ is met with an RNCRN with $M = 6$ chemical perceptrons and coefficients $\beta_1 = \beta_2 = 1, \gamma = 1$, and

$$\boldsymbol{\alpha}_1 = \begin{pmatrix} 0.492 \\ -0.117 \\ 2.229 \\ -0.708 \\ -1.146 \\ 1.363 \end{pmatrix}, \quad \boldsymbol{\alpha}_2 = \begin{pmatrix} -0.283 \\ 0.657 \\ 2.199 \\ -1.294 \\ -2.632 \\ 3.118 \end{pmatrix}, \quad \boldsymbol{\theta} = \begin{pmatrix} 2.243 \\ 10.838 \\ 10.718 \\ -3.164 \\ 7.959 \\ 3.002 \end{pmatrix},$$

$$\boldsymbol{\omega}_1 = \begin{pmatrix} -3.672 \\ 0.911 \\ -1.391 \\ 0.241 \\ -0.454 \\ -0.077 \end{pmatrix}, \quad \boldsymbol{\omega}_2 = \begin{pmatrix} 2.091 \\ -3.981 \\ -1.433 \\ 1.058 \\ -0.922 \\ -0.073 \end{pmatrix}, \quad (28)$$

where $\boldsymbol{\alpha}_i = (\alpha_{i,1}, \alpha_{i,2}, \dots, \alpha_{i,6})^\top$ for $i = 1, 2$, $\boldsymbol{\omega}_i = (\omega_{1,i}, \omega_{2,i}, \dots, \omega_{6,i})^\top$ for $i = 1, 2$, and $\boldsymbol{\theta} =$

$(\theta_1, \theta_2, \dots, \theta_6)^\top$. The reduced ODEs are given by

$$\begin{aligned}\frac{d\tilde{x}_1}{dt} &= g_1(\tilde{x}_1, \tilde{x}_2) = 1 + \tilde{x}_1 \sum_{j=1}^6 \alpha_{1,j} \sigma_1 (\omega_{j,1} \tilde{x}_1 + \omega_{j,2} \tilde{x}_2 + \theta_j), \\ \frac{d\tilde{x}_2}{dt} &= g_2(\tilde{x}_1, \tilde{x}_2) = 1 + \tilde{x}_2 \sum_{j=1}^6 \alpha_{2,j} \sigma_1 (\omega_{j,1} \tilde{x}_1 + \omega_{j,2} \tilde{x}_2 + \theta_j),\end{aligned}\quad (29)$$

while the full ODEs read

$$\begin{aligned}\frac{dx_1}{dt} &= 1 + x_1 \left(\sum_{j=1}^6 \alpha_{1,j} y_j \right), & \frac{dx_2}{dt} &= 1 + x_2 \left(\sum_{j=1}^6 \alpha_{2,j} y_j \right), \\ \mu \frac{dy_1}{dt} &= 1 + \left(\sum_{i=1}^2 \omega_{1,i} x_i + \theta_1 \right) y_1 - y_1^2, & \mu \frac{dy_2}{dt} &= 1 + \left(\sum_{i=1}^2 \omega_{2,i} x_i + \theta_2 \right) y_2 - y_2^2, \\ \mu \frac{dy_3}{dt} &= 1 + \left(\sum_{i=1}^2 \omega_{3,i} x_i + \theta_3 \right) y_3 - y_3^2, & \mu \frac{dy_4}{dt} &= 1 + \left(\sum_{i=1}^2 \omega_{4,i} x_i + \theta_4 \right) y_4 - y_4^2, \\ \mu \frac{dy_5}{dt} &= 1 + \left(\sum_{i=1}^2 \omega_{5,i} x_i + \theta_5 \right) y_5 - y_5^2, & \mu \frac{dy_6}{dt} &= 1 + \left(\sum_{i=1}^2 \omega_{6,i} x_i + \theta_6 \right) y_6 - y_6^2,\end{aligned}\quad (30)$$

Here, we assume general initial concentrations: $x_1(0) = a_1 \in [3.5, 6.5]$, $x_2(0) = a_2 \in [3.5, 6.5]$, and $y_1(0) = b_1 \geq 0$, $y_2(0) = b_2 \geq 0$, $y_3(0) = b_3 \geq 0$, $y_4(0) = b_4 \geq 0$, $y_5(0) = b_5 \geq 0$, and $y_6(0) = b_6 \geq 0$. The coefficients were rounded to 3 decimal places to quote in text, the full precision coefficients are available in the code repository.

Randomly perturbed rates. By randomly perturbing the rate constants in equation (28) with 10% uniform noise we found sets of rate constants that lead to the oscillator dynamical behaviour in a Hopf bifurcation e.g.,

$$\begin{aligned}\boldsymbol{\alpha}_1 &= \begin{pmatrix} 0.532 \\ -0.106 \\ 2.315 \\ -0.693 \\ -1.116 \\ 1.467 \end{pmatrix}, \quad \boldsymbol{\alpha}_2 = \begin{pmatrix} -0.286 \\ 0.645 \\ 1.989 \\ -1.231 \\ -2.614 \\ 3.228 \end{pmatrix}, \quad \boldsymbol{\theta} = \begin{pmatrix} 2.025 \\ 10.419 \\ 11.140 \\ -3.029 \\ 8.754 \\ 3.069 \end{pmatrix}, \\ \boldsymbol{\omega}_1 &= \begin{pmatrix} -3.912 \\ 0.843 \\ -1.345 \\ 0.222 \\ -0.481 \\ -0.083 \end{pmatrix}, \quad \boldsymbol{\omega}_2 = \begin{pmatrix} 2.059 \\ -3.679 \\ -1.552 \\ 1.070 \\ -0.929 \\ -0.075 \end{pmatrix},\end{aligned}\quad (31)$$

and, for completeness, we found examples of unstable behaviour including

$$\begin{aligned}
\boldsymbol{\alpha}_1 &= \begin{pmatrix} 0.493 \\ -0.117 \\ 2.223 \\ -0.711 \\ -1.147 \\ 1.355 \end{pmatrix}, \quad \boldsymbol{\alpha}_2 = \begin{pmatrix} -0.284 \\ 0.657 \\ 2.192 \\ -1.299 \\ -2.609 \\ 3.110 \end{pmatrix}, \quad \boldsymbol{\theta} = \begin{pmatrix} 2.220 \\ 10.930 \\ 10.815 \\ -3.142 \\ 7.890 \\ 2.991 \end{pmatrix}, \\
\boldsymbol{\omega}_1 &= \begin{pmatrix} -3.667 \\ 0.920 \\ -1.396 \\ 0.241 \\ -0.451 \\ -0.077 \end{pmatrix}, \quad \boldsymbol{\omega}_2 = \begin{pmatrix} 2.085 \\ -4.016 \\ -1.432 \\ 1.065 \\ -0.924 \\ -0.073 \end{pmatrix}.
\end{aligned} \tag{32}$$

B Appendix: Piecewise systems

We now present the RNCRNs associated with Section B.

B.1 Simple unistable-bistable piecewise system

We use Algorithm 3, a modified version of Algorithm 1 from [51] with static executive species augmented with automatic differentiation techniques, to approximate the target system (12) on $\mathbb{K}_1 = [1, 9]$ and $\mathbb{L}_1 = \{1\}, \mathbb{L}_2 = \{0\}$ with a parametrized RNCRN. Tolerance $\varepsilon \approx 10^1$ is met with an RNCRN with $M = 3$ chemical perceptrons and coefficients

$$\begin{aligned} \frac{dx_1}{dt} &= 35.700 - 54.403x_1y_1 + 188.696x_1y_2 - 112.261x_1y_3, & x_1(0) &= a_1 \in \mathbb{K}_1, \\ \mu \frac{dy_1}{dt} &= 52.618 + 137.501x_1y_1 - 477.661\lambda_1y_1 - 1513.810y_1 - 90.515y_1^2, & y_1(0) &= b_1 \geq 0, \\ \mu \frac{dy_2}{dt} &= 179.420 - 249.394x_1y_2 - 21494.744\lambda_1y_2 - 220.319y_2 - 12.931y_2^2, & y_2(0) &= b_2 \geq 0, \\ \mu \frac{dy_3}{dt} &= 130.184 - 225.249x_1y_3 - 1876.261\lambda_1y_3 + 854.494y_3 - 1122.973y_3^2, & y_3(0) &= b_3 \geq 0, \\ \frac{d\lambda_1}{dt} &= 0, & \lambda_1(0) &= c_1 \in \mathbb{K}_r. \end{aligned} \quad (33)$$

The reduced vector field of equation (33) is

$$\begin{aligned} \frac{d\tilde{x}_1}{dt} &= 35.700 - 54.403\tilde{x}_1\tilde{y}_1 + 188.696\tilde{x}_1\tilde{y}_2 - 112.261\tilde{x}_1\tilde{y}_3, & x_1(0) &= a_1 \in \mathbb{K}_1, \\ \tilde{y}_1 &= \sigma_{52.618, 90.515}(137.501\tilde{x}_1 - 477.661\tilde{\lambda}_1 - 1513.810), \\ \tilde{y}_2 &= \sigma_{179.420, 12.931}(-249.394\tilde{x}_1 - 21494.744\tilde{\lambda}_1 - 220.319), \\ \tilde{y}_3 &= \sigma_{130.184, 1122.973}(-225.249\tilde{x}_1 - 1876.261\tilde{\lambda}_1 + 854.494), \\ \tilde{\lambda}_1 &= \lambda(0) = c_1 \end{aligned} \quad (34)$$

where the chemical activation function is defined as in equation (66).

B.2 XOR-gated unistable-bistable piecewise system

We used Algorithm 4 to train a classification-controlled RNCRN, i.e. equation (14)-(15), to approximate the more complicated unistable-bistable piecewise systems (17). Intuitively, Algorithm 4 first trains a parametrized RNCRN to approximate a bifurcations between the desired dynamical regimes. Then, a feed-forward network of chemical perceptrons is trained to control the chemical concentration of the bifurcation parameter according to the desired classification boundaries of the environmental species.

In this appendix we walk through the steps of Algorithm 4 in the context of the example target system (17).

Step 1. Point-wise parametrized RNCRN. For ease of demonstration, we use the RNCRN found in Section 4.1. We note from Figure 3(e) that the bifurcation point is approximately at 10^{-2} . Otherwise, apply the step **(a)** from Algorithm 4.

Step 2. Quasi-static classification CRN. We want to create a feed-forward classification that embeds the XOR logic from the target equation (17) into a chemical reaction network and triggers the appropriate dynamical regime. That is, we train a neural CRN to approximate the function

$$\bar{r}(\bar{\lambda}_1, \bar{\lambda}_2) = \begin{cases} 1 & \text{for all } (\bar{\lambda}_1, \bar{\lambda}_2) \in \mathbb{L}_1 = (\mathbb{K}_1 \times \mathbb{K}_2) \cup (\mathbb{K}_2 \times \mathbb{K}_1) \\ 0 & \text{for all } (\bar{\lambda}_1, \bar{\lambda}_2) \in \mathbb{L}_2 = (\mathbb{K}_1 \times \mathbb{K}_1) \cup (\mathbb{K}_2 \times \mathbb{K}_2), \end{cases} \quad (35)$$

where $\mathbb{K}_1 = [0, 1]$ and $\mathbb{K}_2 = [1, 2]$. We define a structure of $K = 4$ chemical perceptrons [56] that catalytically senses the environmental species Λ_1 and Λ_2 . These sense-chemical-perceptrons then feed into a bifurcation species R , which also has a chemical perceptron structure, that will later be connected to the parametrized RNCRN in place of the bifurcation parameter. The corresponding RRE of the aforementioned feed-forward chemical perceptron structure is defined as

$$\begin{aligned} \mu \frac{dz_1}{dt} &= 0.01 + 2.726\lambda_1 z_1 - 3.025\lambda_2 z_1 + 0.296z_1 - z_1^2, & z_1(0) &= c_1 \geq 0, \\ \mu \frac{dz_2}{dt} &= 0.01 + 2.259\lambda_1 z_2 + 0.057\lambda_2 z_2 - 2.328z_2 - z_2^2, & z_2(0) &= c_2 \geq 0, \\ \mu \frac{dz_3}{dt} &= 0.01 - 0.051\lambda_1 z_3 - 2.511\lambda_2 z_3 + 2.582z_3 - z_3^2, & z_3(0) &= c_3 \geq 0, \\ \mu \frac{dz_4}{dt} &= 0.01 + 0.158\lambda_1 z_4 - 0.156\lambda_2 z_4 + 0.666z_4 - z_4^2, & z_4(0) &= c_4 \geq 0, \\ \mu \frac{dr}{dt} &= 0.01 + 4.528z_1 r - 5.719z_2 r - 5.648z_3 r + 0.777z_4 r + 0.682r - r^2, & r(0) &= d \geq 0, \\ \frac{d\lambda_1}{dt} &= 0, & \lambda_1(0) &= e_1 \geq 0, \\ \frac{d\lambda_2}{dt} &= 0, & \lambda_2(0) &= e_2 \geq 0, \end{aligned} \quad (36)$$

where z_1, \dots, z_4 are the time-dependent molecular concentrations of the sense-chemical-perceptron species, λ_1 and λ_2 are the molecular concentrations of the environmental species (which are assumed to be static), and r is the molecular concentration of the bifurcation species. We found these rate constants by training an ANN with the chemical activation function, σ_γ , using standard machine learning methods then mapping the parameters back to the full chemical perceptron RRE with an additional timescale parameter μ .

Step 3. Dynamical approximation. The complete classification-controlled RNCRN is constructed from the combination of the chemical reaction networks that produce reaction-rate equation (33) and reaction-rate equation (36) as shown in Figure 5 the $\mu = 0.001$ parameter was found to be sufficient.

$$\begin{aligned}
\frac{dx_1}{dt} &= 35.700 - 54.403x_1y_1 + 188.696x_1y_2 - 112.261x_1y_3, & x_1(0) &= a_1 \in \mathbb{K}_1, \\
\mu \frac{dy_1}{dt} &= 52.618 + 137.501x_1y_1 - 477.661ry_1 - 1513.810y_1 - 90.515y_1^2, & y_1(0) &= b_1 \geq 0, \\
\mu \frac{dy_2}{dt} &= 179.420 - 249.394x_1y_2 - 21494.744ry_2 - 220.319y_2 - 12.931y_2^2, & y_2(0) &= b_2 \geq 0, \\
\mu \frac{dy_3}{dt} &= 130.184 - 225.249x_1y_3 - 1876.261ry_3 + 854.494y_3 - 1122.973y_3^2, & y_3(0) &= b_3 \geq 0, \\
\mu \frac{dz_1}{dt} &= 0.01 + 2.726\lambda_1z_1 - 3.025\lambda_2z_1 + 0.296z_1 - z_1^2, & z_1(0) &= c_1 \geq 0, \\
\mu \frac{dz_2}{dt} &= 0.01 + 2.259\lambda_1z_2 + 0.057\lambda_2z_2 - 2.328z_2 - z_2^2, & z_2(0) &= c_2 \geq 0, \\
\mu \frac{dz_3}{dt} &= 0.01 - 0.051\lambda_1z_3 - 2.511\lambda_2z_3 + 2.582z_3 - z_3^2, & z_3(0) &= c_3 \geq 0, \\
\mu \frac{dz_4}{dt} &= 0.01 + 0.158\lambda_1z_4 - 0.156\lambda_2z_4 + 0.666z_4 - z_4^2, & z_4(0) &= c_4 \geq 0, \\
\mu \frac{dr}{dt} &= 0.01 + 4.528z_1r - 5.719z_2r - 5.648z_3r + 0.777z_4r + 0.682r - r^2, & r(0) &= d \geq 0, \\
\frac{d\lambda_1}{dt} &= 0, & \lambda_1(0) &= e_1 \geq 0, \\
\frac{d\lambda_2}{dt} &= 0, & \lambda_2(0) &= e_2 \geq 0, \quad (37)
\end{aligned}$$

C Appendix: Example data-defined limit cycles and switching

We now train RNCRNs on training data generated by Algorithm 1 to learn data-defined dynamics. In Figure 9 we emphasize the artificial data generated by Algorithm 1 by showing close-ups of the data used in the examples in Section 5.

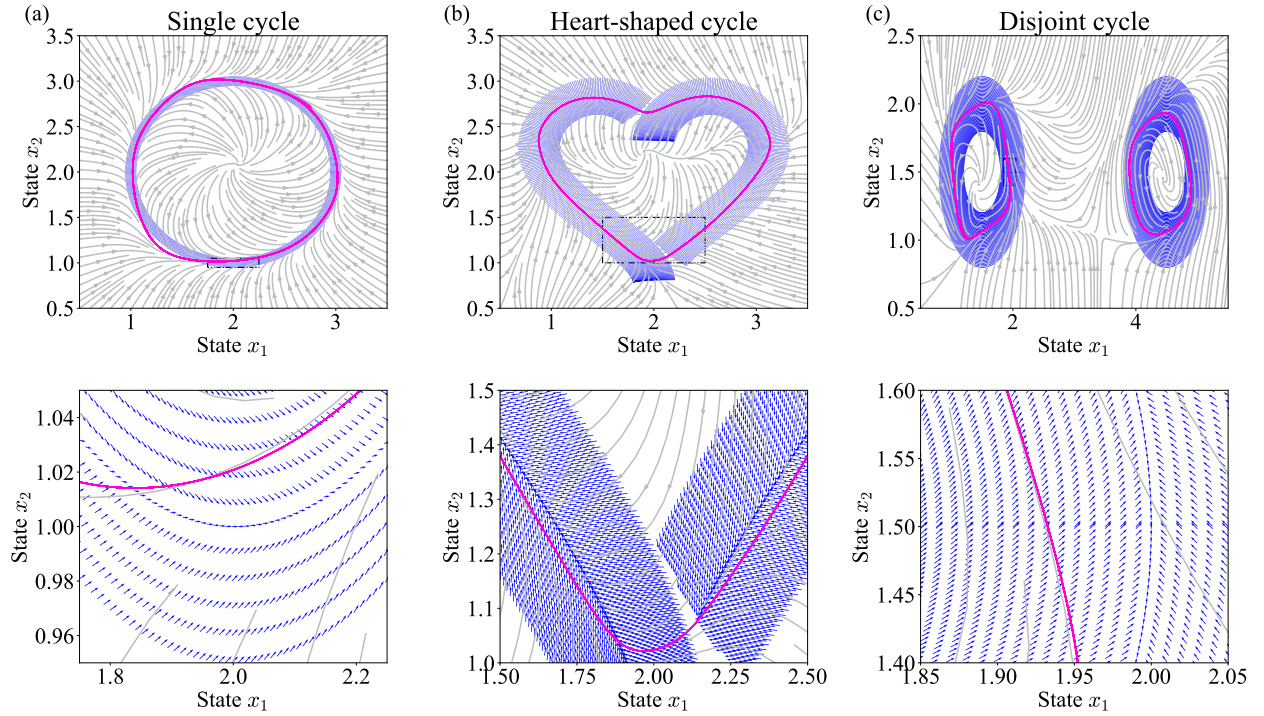


Figure 9: Artificial data used to train the data-defined attractors plotted alongside the reduced vector field (grey) and time-trajectories for the trained RNCRN shown in Figure 6.

C.1 Single circular limit cycle (attractor)

Using the parametric equation defined in Section 5.1, Algorithm 1, and Algorithm 5 we found an RNCRN with $M = 5$ chemical perceptrons and coefficients $\beta_1 = 16.861$, $\beta_2 = 13.955$, and

$$\begin{aligned}
 \boldsymbol{\alpha}_1 &= \begin{pmatrix} -22.642 \\ -3.214 \\ -13.344 \\ -5.983 \\ 11.413 \end{pmatrix}, \quad \boldsymbol{\alpha}_2 = \begin{pmatrix} 20.600 \\ -31.984 \\ 4.736 \\ -9.337 \\ -11.829 \end{pmatrix}, \quad \boldsymbol{\theta} = \begin{pmatrix} 70.437 \\ -86.509 \\ -62.502 \\ 139.089 \\ 77.599 \end{pmatrix}, \\
 \boldsymbol{\omega}_1 &= \begin{pmatrix} -46.744 \\ -21.405 \\ 63.399 \\ -31.199 \\ 20.670 \end{pmatrix}, \quad \boldsymbol{\omega}_2 = \begin{pmatrix} -1.875 \\ 30.682 \\ -47.177 \\ -27.589 \\ -48.644 \end{pmatrix}, \\
 \boldsymbol{\gamma} &= \begin{pmatrix} 22.316 \\ 23.786 \\ 4.064 \\ 0.484 \\ 2.106 \end{pmatrix}, \quad \boldsymbol{\tau} = \begin{pmatrix} 111.885 \\ 106.208 \\ 113.115 \\ 68.879 \\ 94.832 \end{pmatrix}, \tag{38}
 \end{aligned}$$

where $\boldsymbol{\alpha}_i = (\alpha_{i,1}, \alpha_{i,2}, \dots, \alpha_{i,5})^\top$ for $i = 1, 2$, $\boldsymbol{\omega}_i = (\omega_{1,i}, \omega_{2,i}, \dots, \omega_{5,i})^\top$ for $i = 1, 2$, $\boldsymbol{\theta} = (\theta_1, \theta_2, \dots, \theta_5)^\top$, $\boldsymbol{\gamma} = (\gamma_1, \gamma_2, \dots, \gamma_5)^\top$, and $\boldsymbol{\tau} = (\tau_1, \tau_2, \dots, \tau_5)^\top$. The reduced ODEs are given

by

$$\begin{aligned}\frac{d\tilde{x}_1}{dt} &= g_1(\tilde{x}_1, \tilde{x}_2) = 16.861 + \tilde{x}_1 \sum_{j=1}^5 \alpha_{1,j} \sigma_{\gamma_j, \tau_j} (\omega_{j,1} \tilde{x}_1 + \omega_{j,2} \tilde{x}_2 + \theta_j), \\ \frac{d\tilde{x}_2}{dt} &= g_2(\tilde{x}_1, \tilde{x}_2) = 13.955 + \tilde{x}_2 \sum_{j=1}^5 \alpha_{2,j} \sigma_{\gamma_j, \tau_j} (\omega_{j,1} \tilde{x}_1 + \omega_{j,2} \tilde{x}_2 + \theta_j),\end{aligned}\quad (39)$$

while the full ODEs read

$$\begin{aligned}\frac{dx_1}{dt} &= 16.861 + x_1 \left(\sum_{j=1}^5 \alpha_{1,j} y_j \right), & \frac{dx_2}{dt} &= 13.955 + x_2 \left(\sum_{j=1}^5 \alpha_{2,j} y_j \right), \\ \mu \frac{dy_1}{dt} &= 22.316 + \left(\sum_{i=1}^2 \omega_{1,i} x_i + \theta_1 \right) y_1 - 111.885 y_1^2, & \mu \frac{dy_2}{dt} &= 23.786 + \left(\sum_{i=1}^2 \omega_{2,i} x_i + \theta_2 \right) y_2 - 106.208 y_2^2, \\ \mu \frac{dy_3}{dt} &= 4.064 + \left(\sum_{i=1}^2 \omega_{3,i} x_i + \theta_3 \right) y_3 - 113.115 y_3^2, & \mu \frac{dy_4}{dt} &= 0.484 + \left(\sum_{i=1}^2 \omega_{4,i} x_i + \theta_4 \right) y_4 - 68.879 y_4^2, \\ \mu \frac{dy_5}{dt} &= 2.106 + \left(\sum_{i=1}^2 \omega_{5,i} x_i + \theta_5 \right) y_5 - 94.832 y_5^2,\end{aligned}\quad (40)$$

Here, we assume general initial concentrations: $x_1(0) = a_1 > 0$, $x_2(0) = a_2 > 0$, and $y_1(0) = b_1 \geq 0$, $y_2(0) = b_2 \geq 0$, $y_3(0) = b_3 \geq 0$, $y_4(0) = b_4 \geq 0$, and $y_5(0) = b_5 \geq 0$. The coefficients were rounded to 3 decimal places to quote in text, the full precision coefficients are available in the code repository.

C.2 Single circular limit cycle (repeller)

As described in Section 5.1 training data generated by Algorithm 1 (with an inverted normal direction) and equation (18) was used to train an RNCRN using the approach laid out in and Algorithm 5. Figure 10 shows the vector field of the reduced RNCRN approximation of the circular repeller orbit.

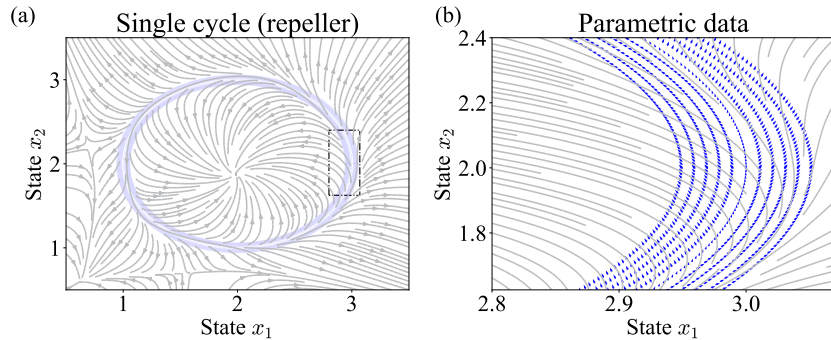


Figure 10: Example RNCRN trained on data to realise a circular repeller. In blue the target repeller data that was created by sampling points from parametric equation (18) then applying a vector field interpolation algorithm, i.e. Algorithm 1. In grey the reduced RNCRN vector field for a 5 chemical perceptron RNCRN (see Appendix C.2 for parameters). Panel (a) shows the entire state-space of interest while panel (b) shows a close-up of the state-space to emphasise the training data.

This training produced an RNCRN with $M = 5$ chemical perceptrons and coefficients $\beta_1 = 81.948$, $\beta_2 = 77.952$, and

$$\begin{aligned} \boldsymbol{\alpha}_1 &= \begin{pmatrix} 43.091 \\ -81.455 \\ -178.720 \\ -6.523 \\ -41.211 \end{pmatrix}, \quad \boldsymbol{\alpha}_2 = \begin{pmatrix} -174.745 \\ -5.587 \\ 51.884 \\ -69.925 \\ -45.358 \end{pmatrix}, \quad \boldsymbol{\theta} = \begin{pmatrix} -306.069 \\ 422.215 \\ -377.697 \\ 445.634 \\ 411.775 \end{pmatrix}, \\ \boldsymbol{\omega}_1 &= \begin{pmatrix} 125.349 \\ -355.600 \\ -354.684 \\ -48.422 \\ -48.630 \end{pmatrix}, \quad \boldsymbol{\omega}_2 = \begin{pmatrix} -404.272 \\ -34.736 \\ 130.538 \\ -344.728 \\ -43.372 \end{pmatrix}, \\ \boldsymbol{\gamma} &= \begin{pmatrix} 87.125 \\ 31.103 \\ 86.664 \\ 26.322 \\ 1.338 \end{pmatrix}, \quad \boldsymbol{\tau} = \begin{pmatrix} 1.719 \\ 236.683 \\ 2.733 \\ 239.852 \\ 488.075 \end{pmatrix}, \end{aligned} \tag{41}$$

where $\boldsymbol{\alpha}_i = (\alpha_{i,1}, \alpha_{i,2}, \dots, \alpha_{i,5})^\top$ for $i = 1, 2$, $\boldsymbol{\omega}_i = (\omega_{1,i}, \omega_{2,i}, \dots, \omega_{5,i})^\top$ for $i = 1, 2$, $\boldsymbol{\theta} = (\theta_1, \theta_2, \dots, \theta_5)^\top$, $\boldsymbol{\gamma} = (\gamma_1, \gamma_2, \dots, \gamma_5)^\top$, and $\boldsymbol{\tau} = (\tau_1, \tau_2, \dots, \tau_5)^\top$. The reduced ODEs are given by

$$\begin{aligned} \frac{d\tilde{x}_1}{dt} &= g_1(\tilde{x}_1, \tilde{x}_2) = 81.948 + \tilde{x}_1 \sum_{j=1}^5 \alpha_{1,j} \sigma_{\gamma_j, \tau_j} (\omega_{j,1} \tilde{x}_1 + \omega_{j,2} \tilde{x}_2 + \theta_j), \\ \frac{d\tilde{x}_2}{dt} &= g_2(\tilde{x}_1, \tilde{x}_2) = 77.952 + \tilde{x}_2 \sum_{j=1}^5 \alpha_{2,j} \sigma_{\gamma_j, \tau_j} (\omega_{j,1} \tilde{x}_1 + \omega_{j,2} \tilde{x}_2 + \theta_j), \end{aligned} \tag{42}$$

while the full ODEs read

$$\begin{aligned} \frac{dx_1}{dt} &= 81.948 + x_1 \left(\sum_{j=1}^5 \alpha_{1,j} y_j \right), & \frac{dx_2}{dt} &= 77.952 + x_2 \left(\sum_{j=1}^5 \alpha_{2,j} y_j \right), \\ \mu \frac{dy_1}{dt} &= 87.125 + \left(\sum_{i=1}^2 \omega_{1,i} x_i + \theta_1 \right) y_1 - 1.719 y_1^2, & \mu \frac{dy_2}{dt} &= 31.103 + \left(\sum_{i=1}^2 \omega_{2,i} x_i + \theta_2 \right) y_2 - 236.683 y_2^2, \\ \mu \frac{dy_3}{dt} &= 86.664 + \left(\sum_{i=1}^2 \omega_{3,i} x_i + \theta_3 \right) y_3 - 2.733 y_3^2, & \mu \frac{dy_4}{dt} &= 26.322 + \left(\sum_{i=1}^2 \omega_{4,i} x_i + \theta_4 \right) y_4 - 239.852 y_4^2, \\ \mu \frac{dy_5}{dt} &= 1.338 + \left(\sum_{i=1}^2 \omega_{5,i} x_i + \theta_5 \right) y_5 - 488.075 y_5^2, \end{aligned} \tag{43}$$

Here, we assume general initial concentrations: $x_1(0) = a_1 > 0$, $x_2(0) = a_2 > 0$, and $y_1(0) = b_1 \geq 0$, $y_2(0) = b_2 \geq 0$, $y_3(0) = b_3 \geq 0$, $y_4(0) = b_4 \geq 0$, and $y_5(0) = b_5 \geq 0$. The coefficients were rounded to 3 decimal places to quote in text, the full precision coefficients are available in the code repository.

C.3 Single circular limit cycle (linear)

As described in the remark in Section 5, Algorithm 1's padding points $Q_{d,k}^\pm$ have the associated vector field $d\mathbf{x}/dt = \eta \hat{v}_{d,d+1} \mp \eta \hat{n}_{d,d+1} \exp(\kappa \delta k)$ with the exponential dependence on the distance

δk . In this example, we show that replacing the exponential dependence with a linear dependence while training the RNCRN can also produce the desired data-defined circular orbit i.e. we use the vector field $d\mathbf{x}/dt = \eta\hat{v}_{d,d+1} \mp \eta\hat{n}_{d,d+1}(\kappa\delta k)$ for padding points.

After generating data with the aforementioned linear modification to Algorithm 1 on the circular equation (18) with $K = 20$, $\delta = 0.01$, $\kappa = 10$, and $\eta = 1$, we trained the RNCRN using Algorithm 5. Figure 11 shows the vector field of the reduced RNCRN approximation of the circular repeller orbit.

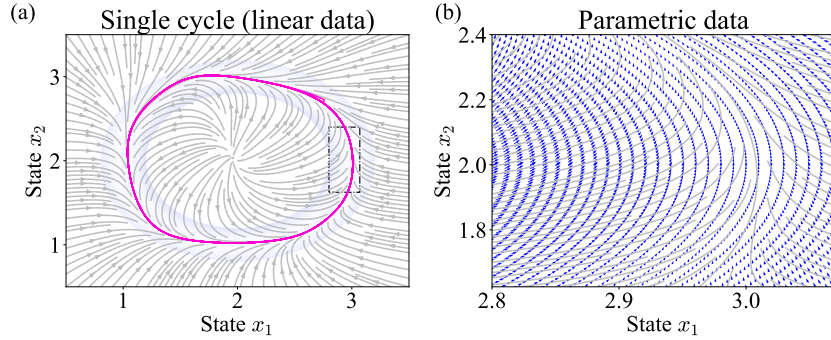


Figure 11: Example RNCRN trained on data to realise a circular attractor using a linear modification of Algorithm 1. In blue the target attractor data was created by sampling points from parametric equation (18) then applying a vector field interpolation algorithm, i.e. Algorithm 1, with a linear modification. In grey the reduced RNCRN vector field for a 5 chemical perceptron RNCRN (see Appendix C.3 for parameters). Panel (a) shows the entire state-space of interest while panel (b) shows a close-up of the state-space to emphasise the training data. The time-trajectory was simulated with $x_1(0) = 2.744$, $x_2(0) = 2.693$, $\mu = 0.1$, and $y_1(0) = \dots, y_5(0) = 0$.

This training produced an RNCRN with $M = 5$ chemical perceptrons and coefficients $\beta_1 = 16.552$, $\beta_2 = 23.165$, and

$$\begin{aligned} \boldsymbol{\alpha}_1 &= \begin{pmatrix} -8.177 \\ -16.814 \\ -21.754 \\ -7.906 \\ 15.501 \end{pmatrix}, \quad \boldsymbol{\alpha}_2 = \begin{pmatrix} 26.539 \\ -22.747 \\ 4.566 \\ -6.631 \\ -30.088 \end{pmatrix}, \quad \boldsymbol{\theta} = \begin{pmatrix} 59.477 \\ -35.099 \\ -60.028 \\ 90.654 \\ 54.644 \end{pmatrix}, \\ \boldsymbol{\omega}_1 &= \begin{pmatrix} -33.517 \\ -28.584 \\ 39.503 \\ -22.314 \\ 0.131 \end{pmatrix}, \quad \boldsymbol{\omega}_2 = \begin{pmatrix} -9.963 \\ 19.259 \\ -40.894 \\ -17.509 \\ -40.181 \end{pmatrix}, \\ \boldsymbol{\gamma} &= \begin{pmatrix} 23.272 \\ 27.928 \\ 8.608 \\ 0.397 \\ 20.500 \end{pmatrix}, \quad \boldsymbol{\tau} = \begin{pmatrix} 56.930 \\ 62.523 \\ 61.866 \\ 36.392 \\ 46.726 \end{pmatrix}, \end{aligned} \tag{44}$$

where $\boldsymbol{\alpha}_i = (\alpha_{i,1}, \alpha_{i,2}, \dots, \alpha_{i,5})^\top$ for $i = 1, 2$, $\boldsymbol{\omega}_i = (\omega_{1,i}, \omega_{2,i}, \dots, \omega_{5,i})^\top$ for $i = 1, 2$, $\boldsymbol{\theta} = (\theta_1, \theta_2, \dots, \theta_5)^\top$, $\boldsymbol{\gamma} = (\gamma_1, \gamma_2, \dots, \gamma_5)^\top$, and $\boldsymbol{\tau} = (\tau_1, \tau_2, \dots, \tau_5)^\top$. The reduced ODEs are given

by

$$\begin{aligned}\frac{d\tilde{x}_1}{dt} &= g_1(\tilde{x}_1, \tilde{x}_2) = 16.552 + \tilde{x}_1 \sum_{j=1}^5 \alpha_{1,j} \sigma_{\gamma_j, \tau_j} (\omega_{j,1}\tilde{x}_1 + \omega_{j,2}\tilde{x}_2 + \theta_j), \\ \frac{d\tilde{x}_2}{dt} &= g_2(\tilde{x}_1, \tilde{x}_2) = 23.165 + \tilde{x}_2 \sum_{j=1}^5 \alpha_{2,j} \sigma_{\gamma_j, \tau_j} (\omega_{j,1}\tilde{x}_1 + \omega_{j,2}\tilde{x}_2 + \theta_j),\end{aligned}\quad (45)$$

while the full ODEs read

$$\begin{aligned}\frac{dx_1}{dt} &= 16.552 + x_1 \left(\sum_{j=1}^5 \alpha_{1,j} y_j \right), & \frac{dx_2}{dt} &= 23.165 + x_2 \left(\sum_{j=1}^5 \alpha_{2,j} y_j \right), \\ \mu \frac{dy_1}{dt} &= 23.272 + \left(\sum_{i=1}^2 \omega_{1,i} x_i + \theta_1 \right) y_1 - 56.930 y_1^2, & \mu \frac{dy_2}{dt} &= 27.928 + \left(\sum_{i=1}^2 \omega_{2,i} x_i + \theta_2 \right) y_2 - 62.523 y_2^2, \\ \mu \frac{dy_3}{dt} &= 8.608 + \left(\sum_{i=1}^2 \omega_{3,i} x_i + \theta_3 \right) y_3 - 61.866 y_3^2, & \mu \frac{dy_4}{dt} &= 0.397 + \left(\sum_{i=1}^2 \omega_{4,i} x_i + \theta_4 \right) y_4 - 36.392 y_4^2, \\ \mu \frac{dy_5}{dt} &= 20.500 + \left(\sum_{i=1}^2 \omega_{5,i} x_i + \theta_5 \right) y_5 - 46.726 y_5^2,\end{aligned}\quad (46)$$

Here, we assume general initial concentrations: $x_1(0) = a_1 > 0$, $x_2(0) = a_2 > 0$, and $y_1(0) = b_1 \geq 0$, $y_2(0) = b_2 \geq 0$, $y_3(0) = b_3 \geq 0$, $y_4(0) = b_4 \geq 0$, and $y_5(0) = b_5 \geq 0$. The coefficients were rounded to 3 decimal places to quote in text, the full precision coefficients are available in the code repository.

C.4 Heart-shaped limit cycle

As described in Section 5.2 training data generated by Algorithm 1 and equation (19) was used to train an RNCRN using Algorithm 5. This training produced an RNCRN with $M = 10$ chemical perceptrons and coefficients $\beta_1 = 32.263$, $\beta_2 = 0.220$, and

$$\begin{aligned}
\boldsymbol{\alpha}_1 &= \begin{pmatrix} -206.685 \\ 68.185 \\ 63.034 \\ 31.454 \\ -1.046 \\ -69.791 \\ 3.335 \\ 6.724 \\ -4.768 \\ -0.753 \end{pmatrix}, \quad \boldsymbol{\alpha}_2 = \begin{pmatrix} 14.421 \\ 361.350 \\ 42.053 \\ -1596.404 \\ 11.659 \\ 445.898 \\ -26.598 \\ 4.145 \\ 9.770 \\ -24.237 \end{pmatrix}, \quad \boldsymbol{\theta} = \begin{pmatrix} 399.866 \\ -2885.359 \\ -3238.521 \\ -4674.896 \\ 1634.028 \\ -2261.417 \\ 1268.967 \\ 1348.322 \\ -2966.115 \\ -965.133 \end{pmatrix}, \\
\boldsymbol{\omega}_1 &= \begin{pmatrix} -752.176 \\ -1404.888 \\ -2126.800 \\ -6923.930 \\ -694.304 \\ -1179.076 \\ 44.345 \\ -472.745 \\ 2317.337 \\ 388.654 \end{pmatrix}, \quad \boldsymbol{\omega}_2 = \begin{pmatrix} -85.831 \\ -2904.666 \\ -3063.465 \\ -3358.036 \\ -126.843 \\ -2667.009 \\ -551.100 \\ -404.818 \\ -1782.721 \\ 29.470 \end{pmatrix}, \\
\boldsymbol{\gamma} &= \begin{pmatrix} 102.958 \\ 317.511 \\ 12.669 \\ 422.712 \\ 0.056 \\ 435.578 \\ 0.572 \\ 0.087 \\ 0.189 \\ 10.109 \end{pmatrix}, \quad \boldsymbol{\tau} = \begin{pmatrix} 735.035 \\ 6155.131 \\ 5217.168 \\ 2052.469 \\ 1814.245 \\ 6080.718 \\ 2388.553 \\ 519.255 \\ 5648.693 \\ 2210.594 \end{pmatrix}, \tag{47}
\end{aligned}$$

where $\boldsymbol{\alpha}_i = (\alpha_{i,1}, \alpha_{i,2}, \dots, \alpha_{i,5})^\top$ for $i = 1, 2$, $\boldsymbol{\omega}_i = (\omega_{1,i}, \omega_{2,i}, \dots, \omega_{5,i})^\top$ for $i = 1, 2$, $\boldsymbol{\theta} = (\theta_1, \theta_2, \dots, \theta_5)^\top$, $\boldsymbol{\gamma} = (\gamma_1, \gamma_2, \dots, \gamma_5)^\top$, and $\boldsymbol{\tau} = (\tau_1, \tau_2, \dots, \tau_5)^\top$. The reduced ODEs are given by

$$\begin{aligned}
\frac{d\tilde{x}_1}{dt} &= g_1(\tilde{x}_1, \tilde{x}_2) = 32.263 + \tilde{x}_1 \sum_{j=1}^{10} \alpha_{1,j} \sigma_{\gamma_j, \tau_j} (\omega_{j,1} \tilde{x}_1 + \omega_{j,2} \tilde{x}_2 + \theta_j), \\
\frac{d\tilde{x}_2}{dt} &= g_2(\tilde{x}_1, \tilde{x}_2) = 0.220 + \tilde{x}_2 \sum_{j=1}^{10} \alpha_{2,j} \sigma_{\gamma_j, \tau_j} (\omega_{j,1} \tilde{x}_1 + \omega_{j,2} \tilde{x}_2 + \theta_j), \tag{48}
\end{aligned}$$

while the full ODEs read

$$\begin{aligned}
\frac{dx_1}{dt} &= 32.263 + x_1 \left(\sum_{j=1}^{10} \alpha_{1,j} y_j \right), & \frac{dx_2}{dt} &= 0.220 + x_2 \left(\sum_{j=1}^{10} \alpha_{2,j} y_j \right), \\
\mu \frac{dy_1}{dt} &= 102.958 + \left(\sum_{i=1}^2 \omega_{1,i} x_i + \theta_1 \right) y_1 - 735.035 y_1^2, & \mu \frac{dy_2}{dt} &= 317.511 + \left(\sum_{i=1}^2 \omega_{2,i} x_i + \theta_2 \right) y_2 - 6155.131 y_2^2, \\
\mu \frac{dy_3}{dt} &= 12.669 + \left(\sum_{i=1}^2 \omega_{3,i} x_i + \theta_3 \right) y_3 - 5217.168 y_3^2, & \mu \frac{dy_4}{dt} &= 422.712 + \left(\sum_{i=1}^2 \omega_{4,i} x_i + \theta_4 \right) y_4 - 2052.469 y_4^2, \\
\mu \frac{dy_5}{dt} &= 0.056 + \left(\sum_{i=1}^2 \omega_{5,i} x_i + \theta_5 \right) y_5 - 1814.245 y_5^2, & \mu \frac{dy_6}{dt} &= 435.578 + \left(\sum_{i=1}^2 \omega_{6,i} x_i + \theta_6 \right) y_6 - 6080.718 y_6^2, \\
\mu \frac{dy_7}{dt} &= 0.572 + \left(\sum_{i=1}^2 \omega_{7,i} x_i + \theta_7 \right) y_7 - 2388.553 y_7^2, & \mu \frac{dy_8}{dt} &= 0.087 + \left(\sum_{i=1}^2 \omega_{8,i} x_i + \theta_8 \right) y_8 - 519.255 y_8^2, \\
\mu \frac{dy_9}{dt} &= 0.189 + \left(\sum_{i=1}^2 \omega_{9,i} x_i + \theta_9 \right) y_9 - 5648.693 y_9^2, & \mu \frac{dy_{10}}{dt} &= 10.109 + \left(\sum_{i=1}^2 \omega_{10,i} x_i + \theta_{10} \right) y_{10} - 2210.594 y_{10}^2,
\end{aligned} \tag{49}$$

Here, we assume general initial concentrations: $x_1(0) = a_1 > 0$, $x_2(0) = a_2 > 0$, and $y_1(0) = b_1 \geq 0$, $y_2(0) = b_2 \geq 0$, $y_3(0) = b_3 \geq 0$, $y_4(0) = b_4 \geq 0$, $y_5(0) = b_5 \geq 0$, $y_6(0) = b_6 \geq 0$, $y_7(0) = b_7 \geq 0$, $y_8(0) = b_8 \geq 0$, $y_9(0) = b_9 \geq 0$, and $y_{10}(0) = b_{10} \geq 0$. The coefficients were rounded to 3 decimal places to quote in text, the full precision coefficients are available in the code repository.

C.5 Multiple limit cycles

As described in Section 5.3 training data generated by Algorithm 1 and equation (18) was used to train an RNCRN using Algorithm 5. This training produced an RNCRN with $M = 15$ chemical

perceptrons and coefficients $\beta_1 = 18.815$, $\beta_2 = 18.135$, and

$$\begin{aligned}
\alpha_1 = & \begin{pmatrix} 0.037 \\ -44.974 \\ -9.160 \\ 0.511 \\ -0.021 \\ 0.567 \\ -4.428 \\ 0.549 \\ -0.238 \\ 0.241 \\ -3.833 \\ -14.058 \\ -0.073 \\ -0.177 \\ 0.025 \end{pmatrix}, \quad \alpha_2 = \begin{pmatrix} 0.053 \\ -35.678 \\ -108.873 \\ 0.039 \\ 0.307 \\ -21.397 \\ 13.701 \\ 0.520 \\ -0.150 \\ -0.041 \\ -11.530 \\ -2.218 \\ 0.108 \\ -0.217 \\ 0.298 \end{pmatrix}, \quad \theta = \begin{pmatrix} -2169.556 \\ -63.584 \\ -63.308 \\ -2110.566 \\ -2062.301 \\ 330.702 \\ 371.345 \\ -2167.958 \\ -2232.450 \\ -2186.657 \\ -2189.514 \\ 366.100 \\ -2077.129 \\ -2345.668 \\ -2176.678 \end{pmatrix}, \\
\omega_1 = & \begin{pmatrix} -2613.137 \\ -133.234 \\ -85.431 \\ -2471.896 \\ -2582.940 \\ -3.890 \\ -85.207 \\ -2593.340 \\ -2869.315 \\ -2738.075 \\ -2545.244 \\ -229.477 \\ -2510.477 \\ -2841.934 \\ -2434.409 \end{pmatrix}, \quad \omega_2 = \begin{pmatrix} -2439.155 \\ 79.236 \\ -283.547 \\ -2319.514 \\ -2296.273 \\ -185.955 \\ -36.065 \\ -2420.028 \\ -2499.550 \\ -2462.773 \\ -2429.244 \\ 4.170 \\ -2312.757 \\ -2641.583 \\ -2347.650 \end{pmatrix}, \\
\gamma = & \begin{pmatrix} 0.046 \\ 48.748 \\ 55.087 \\ 0.047 \\ 0.607 \\ 1.108 \\ 0.359 \\ 0.317 \\ 0.203 \\ 0.087 \\ 0.574 \\ 0.549 \\ 0.069 \\ 0.058 \\ 0.043 \end{pmatrix}, \quad \tau = \begin{pmatrix} 105.841 \\ 632.562 \\ 465.905 \\ 5.862 \\ 114.611 \\ 388.573 \\ 365.923 \\ 28.740 \\ 85.871 \\ 30.612 \\ 2.894 \\ 411.963 \\ 84.905 \\ 75.267 \\ 8.467 \end{pmatrix}, \tag{50}
\end{aligned}$$

where $\boldsymbol{\alpha}_i = (\alpha_{i,1}, \alpha_{i,2}, \dots, \alpha_{i,15})^\top$ for $i = 1, 2$, $\boldsymbol{\omega}_i = (\omega_{1,i}, \omega_{2,i}, \dots, \omega_{15,i})^\top$ for $i = 1, 2$, $\boldsymbol{\theta} = (\theta_1, \theta_2, \dots, \theta_{15})^\top$, $\boldsymbol{\gamma} = (\gamma_1, \gamma_2, \dots, \gamma_{15})^\top$, and $\boldsymbol{\tau} = (\tau_1, \tau_2, \dots, \tau_{15})^\top$. The reduced ODEs are given by

$$\begin{aligned}\frac{d\tilde{x}_1}{dt} &= g_1(\tilde{x}_1, \tilde{x}_2) = 18.815 + \tilde{x}_1 \sum_{j=1}^{15} \alpha_{1,j} \sigma_{\gamma_j, \tau_j} (\omega_{j,1} \tilde{x}_1 + \omega_{j,2} \tilde{x}_2 + \theta_j), \\ \frac{d\tilde{x}_2}{dt} &= g_2(\tilde{x}_1, \tilde{x}_2) = 18.135 + \tilde{x}_2 \sum_{j=1}^{15} \alpha_{2,j} \sigma_{\gamma_j, \tau_j} (\omega_{j,1} \tilde{x}_1 + \omega_{j,2} \tilde{x}_2 + \theta_j),\end{aligned}\quad (51)$$

while the full ODEs read

$$\begin{aligned}\frac{dx_1}{dt} &= 18.815 + x_1 \left(\sum_{j=1}^{10} \alpha_{1,j} y_j \right), & \frac{dx_2}{dt} &= 18.135 + x_2 \left(\sum_{j=1}^{10} \alpha_{2,j} y_j \right), \\ \mu \frac{dy_1}{dt} &= 0.046 + \left(\sum_{i=1}^2 \omega_{1,i} x_i + \theta_1 \right) y_1 - 105.841 y_1^2, & \mu \frac{dy_2}{dt} &= 48.748 + \left(\sum_{i=1}^2 \omega_{2,i} x_i + \theta_2 \right) y_2 - 632.562 y_2^2, \\ \mu \frac{dy_3}{dt} &= 55.087 + \left(\sum_{i=1}^2 \omega_{3,i} x_i + \theta_3 \right) y_3 - 465.905 y_3^2, & \mu \frac{dy_4}{dt} &= 0.047 + \left(\sum_{i=1}^2 \omega_{4,i} x_i + \theta_4 \right) y_4 - 5.862 y_4^2, \\ \mu \frac{dy_5}{dt} &= 0.607 + \left(\sum_{i=1}^2 \omega_{5,i} x_i + \theta_5 \right) y_5 - 114.611 y_5^2, & \mu \frac{dy_6}{dt} &= 1.108 + \left(\sum_{i=1}^2 \omega_{6,i} x_i + \theta_6 \right) y_6 - 388.573 y_6^2, \\ \mu \frac{dy_7}{dt} &= 0.359 + \left(\sum_{i=1}^2 \omega_{7,i} x_i + \theta_7 \right) y_7 - 365.923 y_7^2, & \mu \frac{dy_8}{dt} &= 0.317 + \left(\sum_{i=1}^2 \omega_{8,i} x_i + \theta_8 \right) y_8 - 28.740 y_8^2, \\ \mu \frac{dy_9}{dt} &= 0.203 + \left(\sum_{i=1}^2 \omega_{9,i} x_i + \theta_9 \right) y_9 - 85.871 y_9^2, & \mu \frac{dy_{10}}{dt} &= 0.087 + \left(\sum_{i=1}^2 \omega_{10,i} x_i + \theta_{10} \right) y_{10} - 30.612 y_{10}^2, \\ \mu \frac{dy_{11}}{dt} &= 0.574 + \left(\sum_{i=1}^2 \omega_{11,i} x_i + \theta_{11} \right) y_{11} - 2.894 y_{11}^2, & \mu \frac{dy_{12}}{dt} &= 0.549 + \left(\sum_{i=1}^2 \omega_{12,i} x_i + \theta_{12} \right) y_{12} - 411.963 y_{12}^2, \\ \mu \frac{dy_{13}}{dt} &= 0.069 + \left(\sum_{i=1}^2 \omega_{13,i} x_i + \theta_{13} \right) y_{13} - 84.905 y_{13}^2, & \mu \frac{dy_{14}}{dt} &= 0.058 + \left(\sum_{i=1}^2 \omega_{14,i} x_i + \theta_{14} \right) y_{14} - 75.267 y_{14}^2, \\ \mu \frac{dy_{15}}{dt} &= 0.043 + \left(\sum_{i=1}^2 \omega_{15,i} x_i + \theta_{15} \right) y_{15} - 8.467 y_{15}^2,\end{aligned}\quad (52)$$

Here, we assume general initial concentrations: $x_1(0) = a_1 > 0$, $x_2(0) = a_2 > 0$, and $y_1(0) = b_1 \geq 0$, $y_2(0) = b_2 \geq 0$, $y_3(0) = b_3 \geq 0$, $y_4(0) = b_4 \geq 0$, $y_5(0) = b_5 \geq 0$, $y_6(0) = b_6 \geq 0$, $y_7(0) = b_7 \geq 0$, $y_8(0) = b_8 \geq 0$, $y_9(0) = b_9 \geq 0$, $y_{10}(0) = b_{10} \geq 0$, $y_{11}(0) = b_{11} \geq 0$, $y_{12}(0) = b_{12} \geq 0$, $y_{13}(0) = b_{13} \geq 0$, $y_{14}(0) = b_{14} \geq 0$, and $y_{15}(0) = b_{15} \geq 0$. The coefficients were rounded to 3 decimal places to quote in text, the full precision coefficients are available in the code repository.

C.6 Toroidal limit cycle in three dimensions

Let us now show that Algorithm 1, which is formulated in two dimensions, can be generalized into higher dimensions. In particular, consider the parametric equation for a curve on a torus

$$\begin{aligned}x_1(s) &= 3 \cos(s) + \cos(10s) \cos(s) + 6, \\ x_2(s) &= 3 \sin(s) + \cos(10s) \sin(s) + 6, \\ x_3(s) &= \sin(10s) + 2,\end{aligned}\quad (53)$$

where $s \in [0, 2\pi)$. Figure 12(a) shows three-dimensional training data produced from a generalization of Algorithm 1 to three dimensions. Using this data and Algorithm 5, we train an RNCRN with $M = 7$ chemical perceptrons which, as demonstrated in Figure 12(b), numerically displays a three-dimensional stable limit cycle which is approximately of the desired toroidal shape.

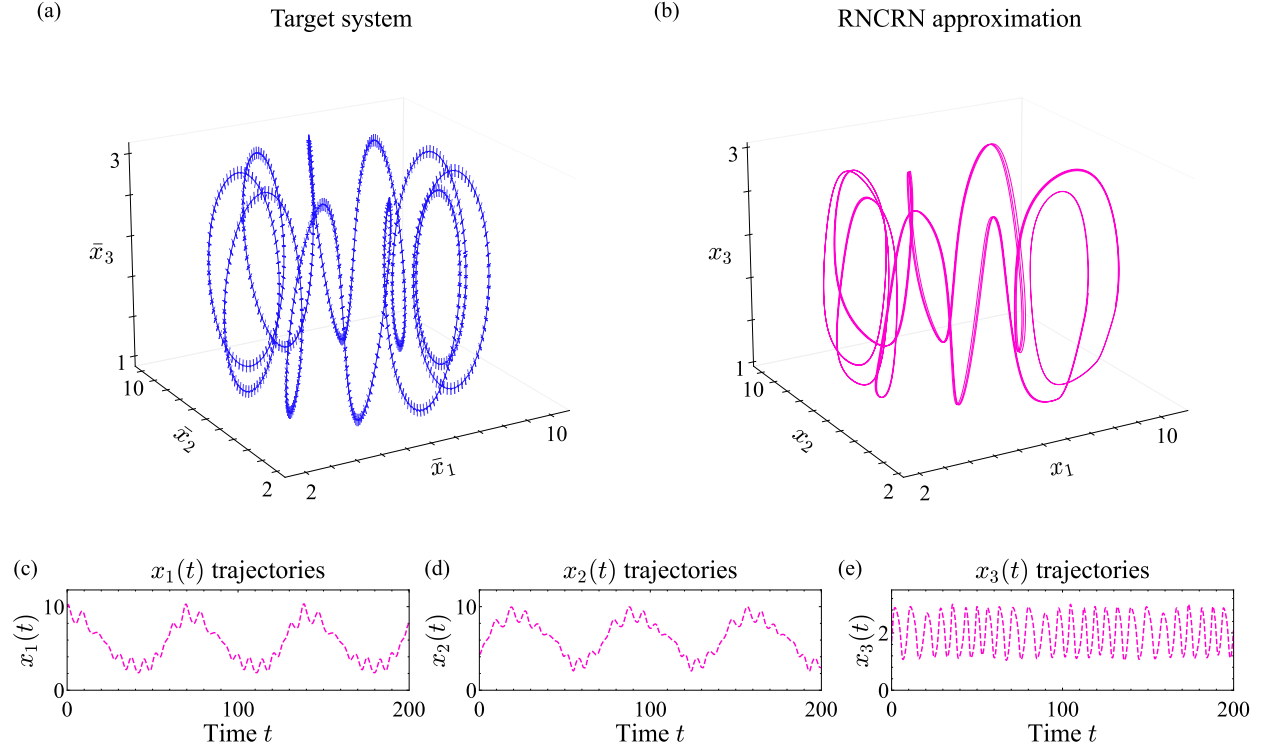


Figure 12: An RNCRN trained to realise a toroidal attractor without an underlying ODE. Panel (a) shows the target attractor data, in blue, that was created by sampling points from parametric equation (53) then applying a modified vector field interpolation algorithm, i.e. Algorithm 1. Panel (b) shows, in magenta, an example state-space trajectory from the $M = 7$ RNCRN approximation with $\mu = 0.01$, $x_1(0) = 10.126$, $x_2(0) = 4.257$, $x_3(0) = 1.703$, and $y_1(0) = \dots, y_7(0) = 0$ (the system is fully specified in Appendix C.6). Panel (c)–(e) show the same trajectory as in panel (b) but in the time-domain for $x_1(t)$, $x_2(t)$, and $x_3(t)$, respectively.

The principal modification was of the data generation algorithm was the generalisation of the placement of padding points into more than one perpendicular direction.

Higher-dimensional data generation. Given a list of points in higher-dimensional $P_d \in \mathbb{R}_{>}^N$ where $N > 2$ we modify Algorithm 1 such that the unit normal from part (a) is replaced with $N - 1$ orthonormal unit vectors that form a basis with the $\hat{v}_{d,d+1}$ direction. Each of these orthonormal unit vectors produce additional padding points and are used to compute the local vector field approximations. To find the orthonormal basis we recognise that a column vector $\hat{v}_{d,d+1} \in \mathbb{R}_{>}^{N \times 1}$ can be decomposed into an orthonormal matrix $Q \in \mathbb{R}_{>}^{N \times N}$ and a scalar $R \in \mathbb{R}$ via QR decomposition where the first column of Q will be linearly dependent on $\hat{v}_{d,d+1}$. It follows that the orthonormal unit vectors are the $N - 1$ remaining column vectors of Q .

RNCRN parameters. Using the higher-dimensional data-generation modification of Algorithm 1 and Algorithm 5 for training, we found an $M = 7$ RNCRN with coefficients $\beta_1 = 1.570$,

$\beta_2 = 0.408$, $\beta_3 = 6.885$, and

$$\begin{aligned}
\boldsymbol{\alpha}_1 &= \begin{pmatrix} -5.227 \\ -6.586 \\ 0.332 \\ -1.297 \\ 1.037 \\ -0.752 \\ 7.607 \end{pmatrix}, \quad \boldsymbol{\alpha}_2 = \begin{pmatrix} -0.755 \\ -5.934 \\ -3.663 \\ 14.209 \\ 1.077 \\ 1.567 \\ 2.768 \end{pmatrix}, \quad \boldsymbol{\alpha}_3 = \begin{pmatrix} 30.463 \\ -19.509 \\ 23.421 \\ -20.966 \\ -45.739 \\ 4.597 \\ 3.169 \end{pmatrix}, \quad \boldsymbol{\theta} = \begin{pmatrix} 292.047 \\ -280.508 \\ 261.422 \\ -255.093 \\ 262.072 \\ -198.768 \\ -139.727 \end{pmatrix}, \\
\boldsymbol{\omega}_1 &= \begin{pmatrix} -39.116 \\ -17.292 \\ -3.625 \\ 7.586 \\ -9.729 \\ 207.473 \\ -109.965 \end{pmatrix}, \quad \boldsymbol{\omega}_2 = \begin{pmatrix} -2.949 \\ -1.592 \\ -36.064 \\ -105.612 \\ -9.325 \\ -327.333 \\ -28.268 \end{pmatrix}, \quad \boldsymbol{\omega}_3 = \begin{pmatrix} -53.870 \\ 111.653 \\ -32.435 \\ 145.520 \\ -67.332 \\ -308.171 \\ 344.645 \end{pmatrix}, \\
\boldsymbol{\gamma} &= \begin{pmatrix} 5.488 \\ 7.535 \\ 3.963 \\ 9.258 \\ 6.007 \\ 0.004 \\ 5.764 \end{pmatrix}, \quad \boldsymbol{\tau} = \begin{pmatrix} 666.189 \\ 812.839 \\ 496.655 \\ 912.664 \\ 428.803 \\ 713.388 \\ 4637.415 \end{pmatrix}, \tag{54}
\end{aligned}$$

where $\boldsymbol{\alpha}_i = (\alpha_{i,1}, \alpha_{i,2}, \dots, \alpha_{i,7})^\top$ for $i = 1, 2, 3$, $\boldsymbol{\omega}_i = (\omega_{1,i}, \omega_{2,i}, \dots, \omega_{7,i})^\top$ for $i = 1, 2, 3$, $\boldsymbol{\theta} = (\theta_1, \theta_2, \dots, \theta_7)^\top$, $\boldsymbol{\gamma} = (\gamma_1, \gamma_2, \dots, \gamma_7)^\top$, and $\boldsymbol{\tau} = (\tau_1, \tau_2, \dots, \tau_7)^\top$. The reduced ODEs are given by

$$\begin{aligned}
\frac{d\tilde{x}_1}{dt} &= g_1(\tilde{x}_1, \tilde{x}_2, \tilde{x}_3) = 1.570 + \tilde{x}_1 \sum_{j=1}^7 \alpha_{1,j} \sigma_{\gamma_j, \tau_j} (\omega_{j,1} \tilde{x}_1 + \omega_{j,2} \tilde{x}_2 + \omega_{j,3} \tilde{x}_3 + \theta_j), \\
\frac{d\tilde{x}_2}{dt} &= g_2(\tilde{x}_1, \tilde{x}_2, \tilde{x}_3) = 0.408 + \tilde{x}_2 \sum_{j=1}^7 \alpha_{2,j} \sigma_{\gamma_j, \tau_j} (\omega_{j,1} \tilde{x}_1 + \omega_{j,2} \tilde{x}_2 + \omega_{j,3} \tilde{x}_3 + \theta_j), \\
\frac{d\tilde{x}_3}{dt} &= g_3(\tilde{x}_1, \tilde{x}_2, \tilde{x}_3) = 6.885 + \tilde{x}_3 \sum_{j=1}^7 \alpha_{3,j} \sigma_{\gamma_j, \tau_j} (\omega_{j,1} \tilde{x}_1 + \omega_{j,2} \tilde{x}_2 + \omega_{j,3} \tilde{x}_3 + \theta_j), \tag{55}
\end{aligned}$$

while the full ODEs read

$$\begin{aligned}
\frac{dx_1}{dt} &= 1.570 + x_1 \left(\sum_{j=1}^7 \alpha_{1,j} y_j \right), & \frac{dx_2}{dt} &= 0.408 + x_2 \left(\sum_{j=1}^7 \alpha_{2,j} y_j \right), \\
\frac{dx_3}{dt} &= 6.885 + x_3 \left(\sum_{j=1}^7 \alpha_{3,j} y_j \right), & \mu \frac{dy_1}{dt} &= 5.488 + \left(\sum_{i=1}^3 \omega_{1,i} x_i + \theta_1 \right) y_1 - 666.189 y_1^2, \\
\mu \frac{dy_2}{dt} &= 7.535 + \left(\sum_{i=1}^3 \omega_{2,i} x_i + \theta_2 \right) y_2 - 812.839 y_2^2, & \mu \frac{dy_3}{dt} &= 3.963 + \left(\sum_{i=1}^3 \omega_{3,i} x_i + \theta_3 \right) y_3 - 496.655 y_3^2, \\
\mu \frac{dy_4}{dt} &= 9.258 + \left(\sum_{i=1}^3 \omega_{4,i} x_i + \theta_4 \right) y_4 - 912.664 y_4^2, & \mu \frac{dy_5}{dt} &= 6.007 + \left(\sum_{i=1}^3 \omega_{5,i} x_i + \theta_5 \right) y_5 - 428.803 y_5^2, \\
\mu \frac{dy_6}{dt} &= 0.004 + \left(\sum_{i=1}^3 \omega_{6,i} x_i + \theta_6 \right) y_6 - 713.338 y_6^2, & \mu \frac{dy_7}{dt} &= 5.764 + \left(\sum_{i=1}^3 \omega_{7,i} x_i + \theta_7 \right) y_7 - 4637.415 y_7^2,
\end{aligned} \tag{56}$$

Here, we assume general initial concentrations: $x_1(0) = a_1 > 0$, $x_2(0) = a_2 > 0$, $x_3(0) = a_3 > 0$, and $y_1(0) = b_1 \geq 0$, $y_2(0) = b_2 \geq 0$, $y_3(0) = b_3 \geq 0$, $y_4(0) = b_4 \geq 0$, $y_5(0) = b_5 \geq 0$, $y_6(0) = b_6 \geq 0$, and $y_7(0) = b_7 \geq 0$. The coefficients were rounded to 3 decimal places to quote in text, the full precision coefficients are available in the code repository.

C.7 Equilibrium-oscillation piecewise system with data-defined oscillations

We now detail the construction of the classification-controlled RNCRNs applied to approximate the equilibrium-oscillation piecewise system with data-defined oscillations (as introduced in Section 5.4). We use the general method to train a classification-controlled RNCRN, as defined in Algorithm 4, with appropriate modification to use data-defined vector fields.

Step 1. Point-wise parametrized RNCRN. Two dynamical states were defined: a cyclic attractor and a stable equilibrium. First, using Algorithm 1 an attractor was generated for a parametric orbit, equation (18), centered on $b_1 = b_2 = 1.5$ with radius $a = 1$. Second, using the ODEs $dx_1/dt = 0.5 - x_1$ and $dx_2/dt = 0.5 - x_2$ the vector field of the stable equilibrium was used over compact subset $\mathbb{K}_1 = [0.01, 3], \mathbb{K}_2 = [0.01, 3]$. Using the associated control points $r_1 = 1$ and $r_2 = 0.1$ a modified Algorithm 3 (i.e. allowing for data-defined vector fields as in Algorithm 5) was used to find a point-wise parameterized RNCRN that bifurcates between the two target dynamics.

The resulting parametrized RNCRN was found with tolerance $\varepsilon \approx 10^{-1}$ met with an RNCRN with $M = 5$ chemical perceptrons and coefficients $\beta_1 = 0.790, \beta_2 = 0.858$,

$$\begin{aligned}
\boldsymbol{\alpha}_1 &= \begin{pmatrix} 89.517 \\ -13.080 \\ 0.321 \\ -98.540 \\ -69.707 \end{pmatrix}, \quad \boldsymbol{\alpha}_2 = \begin{pmatrix} 96.384 \\ -50.709 \\ -24.353 \\ -11.676 \\ -124.643 \end{pmatrix}, \quad \boldsymbol{\theta} = \begin{pmatrix} -1654.188 \\ 578.636 \\ -2579.316 \\ -3291.187 \\ -1568.960 \end{pmatrix}, \quad \boldsymbol{\tau} = \begin{pmatrix} 38.776 \\ 8373.519 \\ 3629.027 \\ 13631.220 \\ 3385.638 \end{pmatrix}, \\
\boldsymbol{\omega}_1 &= \begin{pmatrix} -1357.492 \\ -727.745 \\ -276.335 \\ -2029.546 \\ -239.827 \end{pmatrix}, \quad \boldsymbol{\omega}_2 = \begin{pmatrix} -1128.933 \\ -802.213 \\ 694.332 \\ 295.107 \\ -775.896 \end{pmatrix}, \quad \boldsymbol{\psi} = \begin{pmatrix} 2380.343 \\ 1605.154 \\ 1198.530 \\ 2737.624 \\ -8382.229 \end{pmatrix}, \quad \boldsymbol{\gamma} = \begin{pmatrix} 75.071 \\ 8.557 \\ 5.288 \\ 73.001 \\ 70.181 \end{pmatrix},
\end{aligned} \tag{57}$$

where $\boldsymbol{\alpha}_i = (\alpha_{i,1}, \alpha_{i,2}, \dots, \alpha_{i,5})^\top$ for $i = 1, 2$, $\boldsymbol{\omega}_i = (\omega_{1,i}, \omega_{2,i}, \dots, \omega_{5,i})^\top$ for $i = 1, 2$, $\boldsymbol{\theta} = (\theta_1, \theta_2, \dots, \theta_5)^\top$, $\boldsymbol{\tau} = (\tau_1, \tau_2, \dots, \tau_5)^\top$, $\boldsymbol{\psi} = (\psi_1, \psi_2, \dots, \psi_5)^\top$, and $\boldsymbol{\gamma} = (\gamma_1, \gamma_2, \dots, \gamma_5)^\top$. The reduced ODEs are given by

$$\begin{aligned}\frac{d\tilde{x}_1}{dt} &= g_1(\tilde{x}_1, \tilde{x}_2; \tilde{r}) = \beta_1 + \tilde{x}_1 \sum_{j=1}^5 \alpha_{1,j} \sigma_{\gamma_j, \tau_j} (\omega_{j,1} \tilde{x}_1 + \omega_{j,2} \tilde{x}_2 + \psi_j \tilde{r} + \theta_j), \\ \frac{d\tilde{x}_2}{dt} &= g_2(\tilde{x}_1, \tilde{x}_2; \tilde{r}) = \beta_2 + \tilde{x}_2 \sum_{j=1}^5 \alpha_{2,j} \sigma_{\gamma_j, \tau_j} (\omega_{j,1} \tilde{x}_1 + \omega_{j,2} \tilde{x}_2 + \psi_j \tilde{r} + \theta_j),\end{aligned}\quad (58)$$

while the full ODEs read

$$\begin{aligned}\frac{dx_1}{dt} &= \beta_1 + x_1 \left(\sum_{j=1}^5 \alpha_{1,j} y_j \right), & \frac{dx_2}{dt} &= \beta_2 + x_2 \left(\sum_{j=1}^5 \alpha_{2,j} y_j \right), \\ \mu \frac{dy_1}{dt} &= \gamma_1 + \left(\sum_{i=1}^2 \omega_{1,i} x_i + \psi_1 r + \theta_1 \right) y_1 - \tau_1 y_1^2, & \mu \frac{dy_2}{dt} &= \gamma_2 + \left(\sum_{i=1}^2 \omega_{2,i} x_i + \psi_2 r + \theta_2 \right) y_2 - \tau_2 y_2^2, \\ \mu \frac{dy_3}{dt} &= \gamma_3 + \left(\sum_{i=1}^2 \omega_{3,i} x_i + \psi_3 r + \theta_3 \right) y_3 - \tau_3 y_3^2, & \mu \frac{dy_4}{dt} &= \gamma_4 + \left(\sum_{i=1}^2 \omega_{4,i} x_i + \psi_4 r + \theta_4 \right) y_4 - \tau_4 y_4^2, \\ \mu \frac{dy_5}{dt} &= \gamma_5 + \left(\sum_{i=1}^2 \omega_{5,i} x_i + \psi_5 r + \theta_5 \right) y_5 - \tau_5 y_5^2, & \frac{dr}{dt} &= 0\end{aligned}\quad (59)$$

Here, we assume general initial concentrations: $x_1(0) = a_1 \in [0.01, 3]$, $x_2(0) = a_2 \in [0.01, 3]$, and $y_1(0) = b_1 \geq 0$, $y_2(0) = b_2 \geq 0$, $y_3(0) = b_3 \geq 0$, $y_4(0) = b_4 \geq 0$, $y_5(0) = b_5 \geq 0$, and $r(0) \geq 0$. The coefficients were rounded to 3 decimal places to quote in text, the full precision coefficients are available in the code repository.

Step 2. Quasi-static classification CRN. We now demonstrate the training of the classification component of the classification-controlled RNCRN described in Figure 7(b). We define a target map from the input species Λ_1 to the bifurcation species as

$$\bar{r}(\bar{\lambda}_1) = \begin{cases} 1 & \text{for all } \bar{\lambda}_1 \in [0, 0.25], \\ 0.1 & \text{for all } \bar{\lambda}_1 > 0.25, \end{cases}\quad (60)$$

we approximate the target map, equation (60), by training a small feed-forward neural network with the chemical activation function, σ_γ , i.e.

$$\begin{aligned}\tilde{z}_1 &= \sigma_\gamma \left(\omega_1^{(z)} \tilde{\lambda}_1 + \theta_1^{(z)} \right) \\ \tilde{z}_2 &= \sigma_\gamma \left(\omega_2^{(z)} \tilde{\lambda}_1 + \theta_2^{(z)} \right) \\ \tilde{z}_3 &= \sigma_\gamma \left(\omega_3^{(z)} \tilde{\lambda}_1 + \theta_3^{(z)} \right) \\ \tilde{r} &= \sigma_\gamma \left(\omega_1^{(r)} \tilde{z}_1 + \omega_2^{(r)} \tilde{z}_2 + \omega_3^{(r)} \tilde{z}_3 + \theta_0^{(r)} \right)\end{aligned}\quad (61)$$

an RRE with a steady state equivalent to equation (61) can be constructed at equilibrium from a series of chemical-perceptrons [56]. We introduce the same timescale separation parameter, μ , as in

the RNCRN so that we have the RRE

$$\begin{aligned}
\frac{d\lambda_1}{dt} &= 0, & \lambda_1(0) &\geq 0 \\
\mu \frac{dz_1}{dt} &= \gamma + \left(\omega_1^{(z)} \lambda_1 + \theta_1^{(z)} \right) z_1 - z_1^2, & z_1(0) &= c_1 \geq 0, \\
\mu \frac{dz_2}{dt} &= \gamma + \left(\omega_2^{(z)} \lambda_1 + \theta_2^{(z)} \right) z_2 - z_2^2, & z_2(0) &= c_2 \geq 0, \\
\mu \frac{dz_3}{dt} &= \gamma + \left(\omega_3^{(z)} \lambda_1 + \theta_3^{(z)} \right) z_3 - z_3^2, & z_3(0) &= c_3 \geq 0, \\
\mu \frac{dr}{dt} &= \gamma + \left(\omega_1^{(r)} z_1 + \omega_2^{(r)} z_2 + \omega_3^{(r)} z_3 + \theta_0^{(r)} \right) r - r^2, & r(0) &= d \geq 0. \tag{62}
\end{aligned}$$

Using standard backpropogation techniques [76] to train equation (61) using data sampled from equation (60) we were able to find parameter values $\gamma = 1$, $\omega_1^{(z)} = -3.899$, $\omega_2^{(z)} = -4.832$, $\omega_3^{(z)} = -5.089$, $\theta_1^{(z)} = 10.786$, $\theta_2^{(z)} = 11.864$, $\theta_3^{(z)} = 12.527$, $\omega_1^{(r)} = 5.960$, $\omega_2^{(r)} = -5.255$, $\omega_3^{(r)} = -7.505$, and $\theta_0^{(r)} = 0.436$.

Step 3. Dynamical approximation. We now combined the RREs to form the complete classification-controlled RNCRN. Using the rates constants defined in equation (57) and equation (62) such that the RREs are,

$$\begin{aligned}
\frac{d\lambda_1}{dt} &= 0, & \frac{dx_1}{dt} &= \beta_1 + x_1 \left(\sum_{j=1}^5 \alpha_{1,j} y_j \right), \\
\frac{dx_2}{dt} &= \beta_2 + x_2 \left(\sum_{j=1}^5 \alpha_{2,j} y_j \right), & \mu \frac{dz_1}{dt} &= \gamma + \left(\omega_1^{(z)} \lambda_1 + \theta_1^{(z)} \right) z_1 - z_1^2, \\
\mu \frac{dz_2}{dt} &= \gamma + \left(\omega_2^{(z)} \lambda_1 + \theta_2^{(z)} \right) z_2 - z_2^2, & \mu \frac{dz_3}{dt} &= \gamma + \left(\omega_3^{(z)} \lambda_1 + \theta_3^{(z)} \right) z_3 - z_3^2, \\
\mu \frac{dr}{dt} &= \gamma + \left(\omega_1^{(r)} z_1 + \omega_2^{(r)} z_2 + \omega_3^{(r)} z_3 + \theta_0^{(r)} \right) r - r^2, & \mu \frac{dy_1}{dt} &= \gamma_1 + \left(\sum_{i=1}^2 \omega_{1,i} x_i + \psi_1 r + \theta_1 \right) y_1 - \tau_1 y_1^2, \\
\mu \frac{dy_2}{dt} &= \gamma_2 + \left(\sum_{i=1}^2 \omega_{2,i} x_i + \psi_2 r + \theta_2 \right) y_2 - \tau_2 y_2^2, & \mu \frac{dy_3}{dt} &= \gamma_3 + \left(\sum_{i=1}^2 \omega_{3,i} x_i + \psi_3 r + \theta_3 \right) y_3 - \tau_3 y_3^2, \\
\mu \frac{dy_4}{dt} &= \gamma_4 + \left(\sum_{i=1}^2 \omega_{4,i} x_i + \psi_4 r + \theta_4 \right) y_4 - \tau_4 y_4^2, & \mu \frac{dy_5}{dt} &= \gamma_5 + \left(\sum_{i=1}^2 \omega_{5,i} x_i + \psi_5 r + \theta_5 \right) y_5 - \tau_5 y_5^2. \tag{63}
\end{aligned}$$

The reduced vector field i.e. equation (63) as $\mu \rightarrow 0$ is

$$\begin{aligned}
\tilde{\lambda}_1(t) &= \tilde{\lambda}_1(0), \\
\tilde{z}_1 &= \sigma_\gamma \left(\omega_1^{(z)} \tilde{\lambda}_1 + \theta_1^{(z)} \right) \\
\tilde{z}_2 &= \sigma_\gamma \left(\omega_2^{(z)} \tilde{\lambda}_1 + \theta_2^{(z)} \right) \\
\tilde{z}_3 &= \sigma_\gamma \left(\omega_3^{(z)} \tilde{\lambda}_1 + \theta_3^{(z)} \right) \\
\tilde{r} &= \sigma_\gamma \left(\omega_1^{(r)} \tilde{z}_1 + \omega_2^{(r)} \tilde{z}_2 + \omega_3^{(r)} \tilde{z}_3 + \theta_0^{(r)} \right), \\
\frac{d\tilde{x}_1}{dt} &= g_1(\tilde{x}_1, \tilde{x}_2; r) = 4.251 + \tilde{x}_1 \sum_{j=1}^5 \alpha_{1,j} \sigma_{\gamma_j, \tau_j} (\omega_{j,1} \tilde{x}_1 + \omega_{j,2} \tilde{x}_2 + \psi_j r + \theta_j), \\
\frac{d\tilde{x}_2}{dt} &= g_2(\tilde{x}_1, \tilde{x}_2; r) = 5.494 + \tilde{x}_2 \sum_{j=1}^5 \alpha_{2,j} \sigma_{\gamma_j, \tau_j} (\omega_{j,1} \tilde{x}_1 + \omega_{j,2} \tilde{x}_2 + \psi_j r + \theta_j). \tag{64}
\end{aligned}$$

D Appendix: Training algorithms

We now present various versions of the training algorithms used throughout this manuscript to train single-layer RNCRNs, parameterized RNCRNs, and classification-controlled RNCRNs.

D.1 Algorithm 2. Two-step algorithm for training *parametrized RNCRNs* to approximate bifurcations.

In Section 3 and Appendix A, we present examples of parametrized RNCRN trained by Algorithm 2.

Fix a target system (7), target executive species compact sets $\mathbb{K}_1, \mathbb{K}_2, \dots, \mathbb{K}_N \subset (0, +\infty)$ and target parameter species compact sets $\mathbb{L} \subset (0, +\infty)^L$. Fix also the rate coefficients $\beta_1, \beta_2, \dots, \beta_N \geq 0$ and $\gamma_1, \dots, \gamma_M > 0$ in the parametrized RNCRN system (8).

- (a) **Quasi-static approximation.** Fix a tolerance $\varepsilon > 0$. Fix also the number of perceptrons $M \geq 1$. Using the backpropagation algorithm [76], find the coefficients $\alpha_{i,j}^*, \theta_j^*, \omega_{j,i}^*, \psi_{j,l}^*$ for $i = 1, 2, \dots, N$, $j = 1, 2, \dots, M$, $l = 1, 2, \dots, L$, such that (mean-square) distance between $(f_i(x_1, x_2, \dots, x_N, \lambda_1, \dots, \lambda_L) - \beta_i)/x_i$ and $\sum_{j=1}^M \alpha_{i,j}^* \sigma_{\gamma_j} \left(\sum_{k=1}^N \omega_{j,k}^* x_k + \sum_{l=1}^L \psi_{j,l}^* \lambda_l + \theta_j^* \right)$ is within the tolerance for $(x_1, x_2, \dots, x_N, \lambda_1, \dots, \lambda_L) \in \mathbb{K}_1 \times \mathbb{K}_2 \times \dots \times \mathbb{K}_N \times \mathbb{L}$. If the tolerance ε is not met, then repeat step (a) with $M + 1$.
- (b) **Dynamical approximation.** Substitute $\alpha_{i,j} = \alpha_{i,j}^*$, $\theta_j = \theta_j^*$, $\omega_{j,i} = \omega_{j,i}^*$, $\psi_{j,l} = \psi_{j,l}^*$ into the parametrized RNCRN (8). Fix the initial conditions $x_1(0), x_2(0), \dots, x_M(0) \geq 0$, $y_1(0), y_2(0), \dots, y_M(0) \geq 0$, $(\lambda_1(0), \lambda_2(0), \dots, \lambda_L(0)) \in \mathbb{L}$, and time $T > 0$. Fix also the speed $0 < \mu \ll 1$ of the perceptrons. Numerically solve the target system (7) and the parameterized RNCRN system (8) over the desired interval $[0, T]$. Time $T > 0$ must be such that $\bar{x}_i(t), x_i(t) \in \mathbb{K}_i$ for all $t \in [0, T]$ for $i = 1, 2, \dots, N$. If $\bar{x}_i(t)$ and $x_i(t)$ are sufficiently close according to a desired criterion for all i , then terminate the algorithm. Otherwise, repeat step (b) with a smaller μ . If no desirable μ is found, then go back to step (a) and choose a smaller ε .

Algorithm 2: Algorithm 1 from [51] is modified to include static executive species (i.e. parameter species). In this modified training procedure, $\lambda_1, \dots, \lambda_L$ and $\psi_{j,l}$ are treated as additional inputs to the artificial neural network component of the algorithm in the same way as x_1, \dots, x_M and $\omega_{j,i}$, and then one minimizes over the x_1, \dots, x_M the target functions as usual. This is equivalent to removing any feedback to λ_l and so setting $d\lambda_l/dt = 0$. See the accompanying code examples [77] for more details.

D.2 Algorithm 3. Two-step algorithm for training *parametrized RNCRNs* to approximate piecewise systems.

In Section 4 and Appendix B, we trained example systems using a modified version of Algorithm 2 to approximate piecewise systems. Note, in this section we also trained the *parameterized RNCRN* with automatic differentiation (AD) [78, 79] presented here, for clarity, as Algorithm 3. This expanded algorithm uses the most general form of the parameterized RNCRN

$$\begin{aligned}
 \frac{dx_i}{dt} &= \beta_i + x_i \sum_{j=1}^M \alpha_{i,j} y_j, & \text{for } i = 1, \dots, N, \\
 \frac{d\lambda_l}{dt} &= 0, & \text{for } l = 1, \dots, L, \\
 \frac{dy_j}{dt} &= \frac{\gamma_j}{\mu} + \left(\sum_{i=1}^N \frac{\omega_{j,i}}{\mu} x_i + \sum_{l=1}^L \frac{\psi_{j,l}}{\mu} \lambda_l + \frac{\theta_j}{\mu} \right) y_j - \frac{\tau_j}{\mu} y_j^2, & \text{for } j = 1, \dots, M,
 \end{aligned} \tag{65}$$

where $x_i = x_i(t) \geq 0$, $y_j = y_j(t) \geq 0$, $\lambda_l = \lambda_l(t) = \lambda_l(0) \geq 0$, $\beta_i \geq 0$, $\alpha_{i,j} \in \mathbb{R}$, $\gamma_j > 0$, $\tau_j > 0$, $\omega_{j,i} \in \mathbb{R}$, $\theta_j \in \mathbb{R}$, and $\psi_{j,l} \in \mathbb{R}$.

These AD techniques are just an alternative method for optimizing the reduced vector field so they do not change the conceptual purpose of the quasi-static approximation step. However, they

allow for optimization over more reaction coefficients in the RNCRN. The use of AD techniques allowed the formulation of the optimization function over the reduced vector field directly, *i.e.* $g_i(\tilde{x}_1, \tilde{x}_2, \dots, \tilde{x}_N) \approx f_i(\tilde{x}_1, \tilde{x}_2, \dots, \tilde{x}_N)$ rather than having to optimize over a transformed target vector field $(f_i(\tilde{x}_1, \tilde{x}_2, \dots, \tilde{x}_N) - \beta_i)/\tilde{x}_i \approx \sum_{j=1}^M \alpha_{i,j}^* \sigma_\gamma \left(\sum_{k=1}^N \omega_{j,k}^* \tilde{x}_k + \theta_j^* \right)$. Therefore, several rate constants that we used to fix arbitrarily prior to the quasi-static approximation are now free to be optimized (*i.e.* β_i and γ). Additionally, we allow the constant production reaction, $\gamma_j > 0$, and the self-sequestration reaction, $\tau_j > 0$, to take independent values for each reaction $j = 1, 2, \dots, M$.

Including these new parameters induces a slightly different chemical activation function in the reduced vector field that is defined as

$$\sigma_{\gamma_j, \tau_j}(A) = \frac{1}{2\tau_j} \left(A^2 + \sqrt{A^2 + 4\tau_j \gamma_j} \right). \quad (66)$$

Fix a target system (13), target executive species compact sets $\mathbb{K}_1, \mathbb{K}_2, \dots, \mathbb{K}_N \subset (0, +\infty)$, and the disjoint sets $\mathbb{L}_1, \mathbb{L}_2, \dots, \mathbb{L}_P \subset (0, +\infty)^L$ in the parameter species space corresponding to conditional target functions $f_i^{(1)}, \dots, f_i^{(P)}$.

- (a) **Quasi-static approximation.** Fix a tolerance $\varepsilon > 0$. Fix also the number of perceptrons $M \geq 1$. Using the backpropagation algorithm [76] implemented via automatic differentiation [78], find the coefficients $\alpha_{i,j}^*, \theta_j^*, \omega_{j,i}^*, \psi_{j,l}^*, \beta_i^*, \gamma_j^*, \tau_j^*$ for $i = 1, 2, \dots, N$, $j = 1, 2, \dots, M$, $l = 1, 2, \dots, L$, such that the (mean-square) distance for all $p = 1, \dots, P$ between $f_i^{(p)}(x_1, x_2, \dots, x_N)$ and $\beta_i + x_i \sum_{j=1}^M \alpha_{i,j}^* \sigma_{\gamma_j, \tau_j} \left(\sum_{k=1}^N \omega_{j,k}^* x_k + \sum_{l=1}^L \psi_{j,l}^* \lambda_l + \theta_j^* \right)$ is within the tolerance for $(x_1, x_2, \dots, x_N, \lambda_1, \dots, \lambda_L) \in \mathbb{K}_1 \times \mathbb{K}_2 \times \dots \times \mathbb{K}_N \times \mathbb{L}_p$. If the tolerance ε is not met, then repeat step (a) with $M + 1$.
- (b) **Dynamical approximation.** Substitute $\alpha_{i,j} = \alpha_{i,j}^*$, $\theta_j = \theta_j^*$, $\omega_{j,i} = \omega_{j,i}^*$, $\psi_{j,l} = \psi_{j,l}^*$, $\beta_i = \beta_i^*$, $\gamma_j = \gamma_j^*$, $\tau_j = \tau_j^*$ into the parametrized RNCRN (65). Fix the initial conditions $x_1(0), x_2(0), \dots, x_M(0) \geq 0$, $y_1(0), y_2(0), \dots, y_M(0) \geq 0$, time $T > 0$, and $(\lambda_1(0), \lambda_2(0), \dots, \lambda_L(0))$ in any \mathbb{L}_p . Fix also the speed $0 < \mu \ll 1$ of the perceptrons. Numerically solve the target system (13) and the parameterized RNCRN system (65) over the desired interval $[0, T]$. Time $T > 0$ must be such that $\bar{x}_i(t), x_i(t) \in \mathbb{K}_i$ for all $t \in [0, T]$ for $i = 1, 2, \dots, N$. If $\bar{x}_i(t)$ and $x_i(t)$ are sufficiently close according to a desired criterion for all i , then terminate the algorithm. Otherwise, repeat step (b) with a smaller μ . If no desirable μ is found, then go back to step (a) and choose a smaller ε .

Algorithm 3: Two-step algorithm for training the *parametrized RNCRN* to approximate piecewise systems. See the accompanying code examples [77] for more details.

D.3 Algorithm 4. Algorithm for training the *classification-controlled RNCRN*.

Fix a target system (13), target executive species compact sets $\mathbb{K}_1, \mathbb{K}_2, \dots, \mathbb{K}_N \subset (0, +\infty)$, and the disjoint sets $\mathbb{L}_1, \mathbb{L}_2, \dots, \mathbb{L}_P \subset (0, +\infty)^L$ in the parameter species space corresponding to conditional target functions $f_i^{(1)}, \dots, f_i^{(P)}$.

- (a) **Point-wise parametrized RNCRN.** Apply Algorithm 3 to find a $L = 1$ parametrized RNCRN that bifurcates between the P conditional target functions using P points, r_1, \dots, r_p , selected arbitrarily from $(0, +\infty)$. Substitute the resulting parameters into (14) as $\alpha_{i,j} = \alpha_{i,j}$, $\theta_j^{(y)} = \theta_j$, $\omega_{j,i}^{(y)} = \omega_{j,i}$, $\psi_j = \psi_{j,1}$, $\beta_i = \beta_i$, $\gamma_j = \gamma_j$, and $\tau_j = \tau_j$.
- (b) **Quasi-static classification CRN.** Fix a tolerance $\varepsilon > 0$. Fix also the number of perceptrons $K \geq 1$ and $\gamma > 0$. Using the backpropagation algorithm [76] find the coefficients $\omega_{k,l}^{*(z)}, \theta_k^{*(z)}, \omega_k^{*(r)}, \theta_0^{*(r)}$ for $l = 1, 2, \dots, L$, $k = 1, 2, \dots, K$, such that (mean-square) distance between r_p and $\sigma_\gamma \left(\sum_{k=1}^K \omega_k^{*(r)} \sigma_\gamma \left(\sum_{l=1}^L \omega_{k,l}^{*(z)} \lambda_l + \theta_k^{*(z)} \right) + \theta_0^{*(r)} \right)$ is within the tolerance for all for all $(\lambda_1, \dots, \lambda_L) \in \mathbb{L}_p$ for all $p = 1, \dots, P$. If the tolerance ε is not met, then repeat step (b) with $K + 1$.
- (c) **Dynamical approximation.** Substitute $\omega_{k,l}^{(z)} = \omega_{k,l}^{*(z)}, \theta_k^{(z)} = \theta_k^{*(z)}, \omega_k^{(r)} = \omega_k^{*(r)}, \theta_0^{(r)} = \theta_0^{*(r)}$ into (15) and couple with (14) with parameters found in (a). Fix the initial conditions $x_1(0), x_2(0), \dots, x_M(0) \geq 0$, $y_1(0), y_2(0), \dots, y_M(0) \geq 0$, $z_1(0), z_2(0), \dots, z_K(0) \geq 0$, $r(0) \geq 0$, time $T > 0$, and $(\lambda_1(0), \lambda_2(0), \dots, \lambda_L(0))$ in any \mathbb{L}_p . Fix also the speed $0 < \mu \ll 1$ of the perceptrons. Numerically solve the target system (13) and the classification-controlled RNCRN system (14)–(15) over the desired interval $[0, T]$. Time $T > 0$ must be such that $\bar{x}_i(t), x_i(t) \in \mathbb{K}_i$ for all $t \in [0, T]$ for $i = 1, 2, \dots, N$. If $\bar{x}_i(t)$ and $x_i(t)$ are sufficiently close according to a desired criterion for all i , then terminate the algorithm. Otherwise, repeat step (b) with a smaller μ . If no desirable μ is found, then go back to step (a) and choose a smaller ε .

Algorithm 4: An algorithm to train *classification-controlled RNCRN* to approximate piecewise systems of the form (13). See the accompanying code examples [77] for more details.

D.4 Algorithm 5. Two-step algorithm for training the *RNCRN* to approximate data-defined limit cycles.

In Section 5 and Appendix C, we trained example systems using a modified versions of Algorithm 1 from [51] on data from Algorithm 1 in this manuscript. For clarity, we present this as Algorithm 5 and note it involved both automatic differentiation techniques and, due to not having an ODE system to validate trajectories, an abridged dynamical approximation step with an informal inspection-based termination.

We allow the constant production reaction, $\gamma_j > 0$, and the self-sequestration reaction, $\tau_j > 0$,

to take independent values for each reaction $j = 1, 2, \dots, M$. The full RNCRN in this situation is

$$\begin{aligned} \frac{dx_i}{dt} &= \beta_i + x_1 \sum_{j=1}^M \alpha_{i,j} y_j, & x_i(0) &= a_i, & \text{for } i = 1, \dots, N, \\ \frac{dy_j}{dt} &= \frac{\gamma_j}{\mu} + \left(\sum_{i=1}^N \frac{\omega_{j,i}}{\mu} x_i + \frac{\theta_j}{\mu} \right) y_j - \frac{\tau_j}{\mu} y_j^2, & y_j(0) &= b_j, & \text{for } j = 1, \dots, M. \end{aligned} \quad (67)$$

Including these new parameters induces a slightly different chemical activation function in the reduced vector field that is defined as in (66).

Fix target data generated by Algorithm 1 (or otherwise) as $\mathbb{X} = \{X^{(1)}, \dots, X^{(D+1)}\}$, the set of points in executive species space, and $\dot{\mathbb{X}} = \{\dot{X}^{(1)}, \dots, \dot{X}^{(D+1)}\}$, the associated vector field for each point. Where $X^{(d)} \in \mathbb{R}_{\geq 0}^N$ and $\dot{X}^{(d)} \in \mathbb{R}^N$ for $d = 1, 2, \dots, D+1$ and $i = 1, 2, \dots, N$.

- (a) **Quasi-static approximation.** Fix a tolerance $\varepsilon > 0$. Fix also the number of perceptrons $M \geq 1$. Using the backpropagation algorithm [76] implemented via automatic differentiation [78], find the coefficients $\alpha_{i,j}^*, \theta_j^*, \omega_{j,i}^*, \beta_i^*, \gamma_j^*, \tau_j^*$ for $i = 1, 2, \dots, N$, $j = 1, 2, \dots, M$, such that (mean-square) distance between $\dot{X}_i^{(d)}$ and $\beta_i + x_i^{(d)} \sum_{j=1}^M \alpha_{i,j}^* \sigma_{\gamma_j, \tau_j} \left(\sum_{k=1}^N \omega_{j,k}^* x_k^{(d)} + \theta_j^* \right)$ is within the tolerance for all for $d = 1, 2, \dots, D+1$ and $i = 1, 2, \dots, N$. If the tolerance ε is not met, then repeat step (a) with $M + 1$.
- (b) **Dynamical approximation.** Substitute $\alpha_{i,j} = \alpha_{i,j}^*$, $\theta_j = \theta_j^*$, $\omega_{j,i} = \omega_{j,i}^*$, $\beta_i = \beta_i^*$, $\gamma_j = \gamma_j^*$, $\tau_j = \tau_j^*$ into the RNCRN (67). Fix the initial conditions $x_1(0), x_2(0), \dots, x_M(0) \geq 0$, $y_1(0), y_2(0), \dots, y_M(0) \geq 0$, and time $T > 0$. Fix also the speed $0 < \mu \ll 1$ of the perceptrons. Numerically solve the RNCRN system (67) over the desired interval $[0, T]$. If, by inspection, the time-trajectory implements the intended dynamics then terminate the algorithm. Otherwise, repeat step (b) with a smaller μ . If no desirable μ is found, then go back to step (a) and choose a smaller ε .

Algorithm 5: An algorithm for training an RNCRN to approximate dynamics from vector field data. Termination of this algorithm is based on an informal inspection of the time-trajectories as there is no ground-truth time-trajectories for these systems. See the accompanying code examples [77] for more details.